JOURNAL OF PETROLOGY | VOLUME 48 | NUMBER 4 | PAGES 729–752 | 2007 | doi:10.1093/petrology/egl080

Lamproitic Rocks from a Continental Collision Zone: Evidence for Recycling of Subducted Tethyan Oceanic Sediments in the Mantle Beneath Southern Tibet

YONGFENG GAO[1]*, ZENGQIAN HOU[2], BALZ S. KAMBER[3], RUIHUA WEI[1], XIANGJIN MENG[4] AND RONGSHENG ZHAO[5]

[1]DEPARTMENT OF RESOURCES, SHIJIAZHUANG UNIVERSITY OF ECONOMICS, HUAIAN EAST ROAD 136, SHIJIAZHUANG, HEBEI 050031, CHINA

[2]INSTITUTE OF GEOLOGY, CHINESE ACADEMY OF SCIENCES, BEIJING 100037, CHINA

[3]DEPARTMENT OF EARTH SCIENCES, LAURENTIAN UNIVERSITY, SUDBURY, ONT., CANADA

[4]INSTITUTE OF MINERAL RESOURCES, CHINESE ACADEMY OF GEOLOGICAL SCIENCES, BEIJING 100037, CHINA

[5]HEBEI BUREAU OF LAND AND RESOURCES, SHIJIAZHUANG, HEBEI 050051, CHINA

RECEIVED FEBRUARY 9, 2005; ACCEPTED DECEMBER 21, 2006; ADVANCE ACCESS PUBLICATION FEBRUARY 22, 2007

Major and trace element, Sr–Nd–Pb isotope and mineral chemical data are presented for newly discovered ultrapotassic lavas in the Tangra Yumco–Xuruco graben in southern Tibet. The ultrapotassic lavas are characterized by high MgO, K_2O and TiO_2, low Al_2O_3 and Na_2O contents, and also have high molar K_2O/Al_2O_3, molar $(K_2O+Na_2O)/Al_2O_3$ and K_2O/Na_2O ratios. Their high abundances of incompatible trace elements such as large ion lithophile elements (LILE) and light rare earth elements (LREE) reach the extreme levels typical of lamproites. The lamproites show highly radiogenic $^{87}Sr/^{86}Sr$ (0·7166–0·7363) and unradiogenic $^{143}Nd/^{144}Nd$ (0·511796–0·511962), low $^{206}Pb/^{204}Pb$ (18·459–18·931), and elevated radiogenic $^{207}Pb/^{204}Pb$ (15·6732–15·841) and $^{208}Pb/^{204}Pb$ (39·557–40·058) ratios. On the basis of their geochemical and isotopic systematics, the lamproites in south Tibet have a distinct magma source that can be differentiated from the sources of potassic lavas in the east Lhasa and Qiangtang blocks. Their high Nb/Ta ratios (17·10–19·84), extremely high Th/U ratios (5·70–13·74) and distinctive isotope compositions are compatible with a veined mantle source consisting of partial melts of subducted Tethyan oceanic sediments and sub-continental lithospheric depleted mantle. Identification of the lamproites and the delineation of their mantle source provide new evidence relevant for models of the uplift and extension of the Tibetan plateau following the Indo-Asia collision. Metasomatism by partial melts from isotopically evolved, old sediment subducted on the young Tethyan slab is an alternative explanation for Precambrian Nd and Pb model ages. In this model, differences in isotopic composition along-strike are attributed to differences in the type of sediment being subducted, thus obviating the need for multiple metasomatic events over hundreds of million years. The distribution of lamproites, restricted within a north–south-trending graben, indicates that the initiation of east–west extension in south Tibet started at ~25 Ma.

KEY WORDS: *lamproites; subducted oceanic sediment; Tibetan active continental collision belt*

INTRODUCTION

The processes responsible for the uplift and extension of the Tibetan plateau following the Indo-Asia collision have long been the subject of debate (e.g. Yin, 2000). Proposed models for the geodynamic evolution of the Tibetan plateau include convective removal of sub-continental lithospheric mantle (SCLM; Houseman *et al.*, 1981; Turner *et al.*, 1993, 1996;

*Corresponding author. Telephone: 0086 311 87207857. Fax: 0086 311 85882537. E-mail: gaoyf@sjzue.edu.cn

Published by Oxford University Press (2007).

Downloaded from http://petrology.oxfordjournals.org/ at Pendlebury Library of Music on November 16, 2014

Williams *et al.*, 2001, 2004), slab break-off (Miller *et al.*, 1999; DeCellers *et al.*, 2002; Kohn & Parkinson, 2002; Mahéo *et al.*, 2002), and intracontinental subduction (Arnaud *et al.*, 1992; Meyer *et al.*, 1998; Tapponnnier *et al.*, 2001; Ding *et al.*, 2003; Guo *et al.*, 2006). Of critical importance for the evaluation of these models is their prediction of the spatial and temporal distribution of post-collisional magmatism on the Tibetan plateau, the duration and conditions of partial melting, and the nature and location of the magma source regions.

Widespread Neogene potassic and ultrapotassic volcanism in southern Tibet has been interpreted as the product of partial melting induced by convective thinning of the lithosphere beneath the Tibetan plateau (Turner *et al.*, 1996; Williams *et al.*, 2001, 2004; Chung *et al.*, 2005). The magmas were considered to be derived from distinct SCLM sources (Turner *et al.*, 1993, 1996; Miller *et al.*, 1999; Williams *et al.*, 2001, 2004). To account for their Nd–Sr–Pb isotopic signatures, it has been suggested that the Tibetan mantle lithosphere experienced a multi-stage history of metasomatism during Precambrian times, as inferred from Neoproterozoic Nd (0·9–1·3 Ga) and even older Pb (2·2–3·5 Ga) model ages (Miller *et al.*, 1999). However, the probability that enriched Precambrian mantle lithosphere has remained chemically isolated and physically intact beneath Tibet for almost 1 Gyr appears unlikely when the complex Phanerozoic tectonic and magmatic evolution of Tibet is considered (Ding *et al.*, 2003). As an alternative, Ding *et al.* (2003) proposed that the Tibetan mantle lithosphere could have been metasomatized much more recently (during Cenozoic times) by fluids or melts derived from ancient continental crust subducted beneath Tibet during the Indo-Asian collision. In their model, the Precambrian Nd and Pb model ages inferred for the Tibetan mantle lithosphere may reflect not the time when the lithosphere became isolated from asthenospheric convection, but rather inheritance of the isotopic signatures from fluids and melts derived from subducted ancient continental crust. One possible problem with this interpretation is that potassic volcanism in the Lhasa block appears to have started before the collision of the Indian continent (Coulon *et al.*, 1986), hence before continental crust could have reached a depth to contribute to magmatism.

In our view, there is one central observation that helps to constrain the source of the ultrapotassic magmatism. Here we draw attention to the fact that true ultrapotassic rocks have chemical and isotopic characteristics that are distinct from those of the potassic volcanic rocks. The ultrapotassic lavas from the Lhasa block may therefore have a distinct, well-defined magma source. Miller *et al.* (1999) suggested that the post-collisional ultrapotassic lavas in SW Tibet have a clear affinity with lamproites from SE Spain and were derived from a separate region of the SCLM. We report major and trace element and Sr–Nd–Pb isotope data for newly discovered outcrops of ultrapotassic lavas from the Tangra Yumco–Xuruco graben in southern Tibet. The samples are chemically identical to the post-collisional ultrapotassic volcanic rocks previously identified from all over the Lhasa block (Miller *et al.*, 1999; Williams *et al.*, 2001, 2004; Ding *et al.*, 2003; Nomade *et al.*, 2004), and, therefore, are likely to be cogenetic. The objectives of this study are to define their petrological and geochemical characteristics, and to provide constraints on their mantle source. Our new data suggest that these lavas are geochemically distinct lamproites, and represent the first examples of lamproite magmas identified from the Tibetan continental collision zone.

GEOLOGICAL SETTING

The geodynamic setting of southern Tibet is particularly complex, as a result of the convergence between the Indian and Asian plates. From the mid-Miocene (25 Ma), there was a renewal of magmatic activity ~25 Myr after the Indo-Asian collision (Mahéo *et al.*, 2002). Since then, the Lhasa block has become the site of widespread, but small-volume, eruptions of ultrapotassic–potassic lavas, adakites and a lesser amount of more felsic magmas (Mahéo *et al.*, 2002; Gao *et al.*, 2003). In spite of the fact that post-collisional potassic volcanic rocks are widespread in the Lhasa terrane (e.g. Xungba, East Jarga, Shiquanhe, Namling, Maquiang, Daggyai Tso, Pabbai Zong, Zabuye, Wuyu, Dajia Co; Turner *et al.*, 1996; Miller *et al.*, 1999; Williams *et al.*, 2001, 2004; Zhao *et al.*, 2001; Ding *et al.*, 2003; Nomade *et al.*, 2004), there are only few outcrops of true ultrapotassic rocks, restricted to the western part of the Lhasa block (Fig. 1).

The recent tectonic style in southern Tibet is marked by north–south-trending normal faults and grabens accommodating east–west extension (Molnar & England, 1978). The Tangra Yumco–Xuruco graben is one of a series of north–south-trending rifts cutting across the Lhasa block within the western part (Figs 1 and 2). The graben is about 300 km long and 40 km wide. North–south-trending active fault belts limit both its eastern and western margins. Two lakes (Tangra Yumco and Xuruco) lie within the rift. The flanks of the rift are dominated by widespread outcrops of voluminous Linzizong volcanic rocks and contemporaneous granitoid intrusions. Isolated occurrences of ultrapotassic–potassic lavas are associated with the rift flanks (Fig. 2). The total area with an ultrapotassic–potassic lava cover is more than 150 km^2. Potassic lavas occur close to Chazi in the southern segment of the rift (Fig. 2); these have an $^{40}Ar/^{39}Ar$ age range from 13·3 ± 0·4 Ma to 8·2 ± 0·5 Ma (Ding *et al.*, 2003). Two occurrences of ultrapotassic lavas are located at Chazi and Mibale, respectively (Fig. 2). The Chazi ultrapotassic lavas occur on the eastern flanks of the rift, and overlie Linzizong volcanic rocks. There are no

Downloaded from http://petrology.oxfordjournals.org/ at Pendlebury Library of Music on November 16, 2014

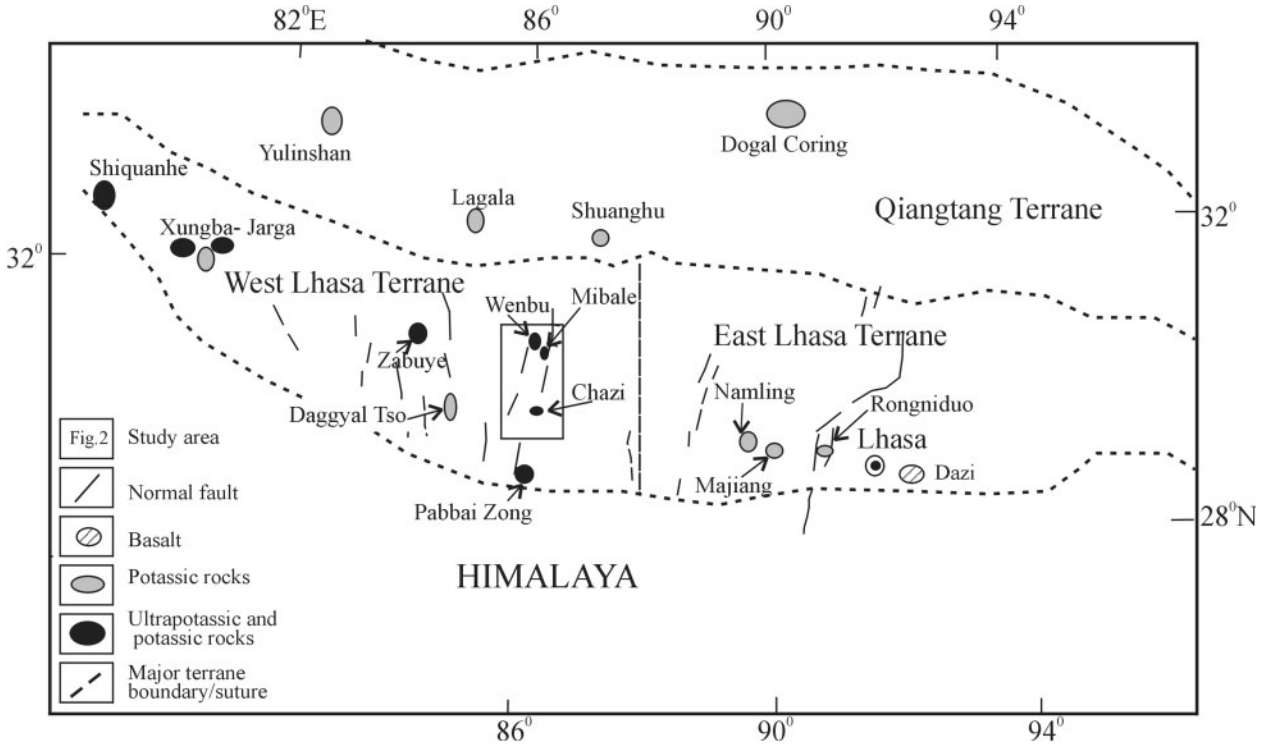


Fig. 1. Simplified map of southern Tibet showing the major terranes and spatial distribution of ultrapotassic and potassic rocks. Data from Coulon *et al.* (1986), Turner *et al.* (1993, 1996), Miller *et al.* (1999), Williams *et al.* (2001, 2004), Zhao *et al.* (2001), Ding *et al.* (2003), Nomade *et al.* (2004) and Gao *et al.* (2006). Rectangle indicates the location of the study area.

exposed field relationships between the Chazi ultrapotassic lavas and the nearby potassic lavas. The Mibale ultrapotassic lavas are underlain by sandstones of the Cretaceous Jingzhushan Formation, and also occur on the eastern flanks of the rift (Fig. 2). These lavas have yielded a K–Ar age of 19·04 ± 0·97 Ma (Liao *et al.*, 2002). A third occurrence of ultrapotassic lavas is a volcanic 'neck' at Wenbu on the western side of the rift, which has yielded $^{40}Ar/^{39}Ar$ sanidine ages from 21·5 ± 0·3 Ma to 17·8 ± 0·3 Ma (Ding *et al.*, 2003). It should be noted that all these geochronological data are consistent with the age range (18–13 Ma) of north–south-trending ultrapotassic dykes at the southern end of the rift (Williams *et al.*, 2001).

ANALYTICAL METHODS

Only fresh rock samples, visibly free of alteration, were selected for analysis. Major elements were determined by gravimetry (wet chemistry) and atomic absorption spectrometry (AAS). Sr and Nd isotope compositions of powered samples were obtained by thermal ionization mass spectrometry (TIMS) (MAT-262) at the Isotope Geology Laboratory, Chinese Academy of Geological Science (Beijing). Repeat measurements of NBS987 yielded $^{87}Sr/^{86}Sr = 0·71025 \pm 2$ (2σ) and the accuracy of the Rb/Sr ratio was better than 0·1% (four repeats). Strontium isotope mass fractionation was corrected using $^{88}Sr/^{86}Sr = 8·37521$. The mean $^{143}Nd/^{144}Nd$ ratio in J&M metal yielded 0·511125 ± 8 (2σ), and the accuracy of the Sm/Nd ratio was better than 0·1% (six repeats). Neodymium isotope fractionation was corrected using $^{146}Nd/^{144}Nd = 0·7219$. Initial ε_{Nd} values and $^{87}Sr/^{86}Sr$ ratios were calculated for an age (t) = 19 Ma. Pb-isotope ratios were determined by strictly pyrometer-controlled TIMS from Pb purified with miniaturized HBr–HCl chemistry from an aliquot of the trace element digestion. The reproducibility of the NBS SRM 981 standard was: $^{206}Pb/^{204}Pb = 16·942 \pm 0·008$; $^{207}Pb/^{204}Pb = 15·496 \pm 0·011$; $^{208}Pb/^{204}Pb = 36·716 \pm 0·036$; $^{207}Pb/^{206}Pb = 0·914622 \pm 0·00018$; $^{208}Pb/^{206}Pb = 2·16714 \pm 0·0011$.

For trace element and Pb isotope compositions, a crushed aliquot was powdered in an agate mill. Trace element concentrations were obtained by solution inductively coupled plasma-mass spectrometry (ICP-MS) at ACQUIRE, University of Queensland, following the analytical procedure described by Kamber *et al.* (2003). The compositions of phenocryst minerals in three samples were determined using a CAMECA SX51 electron microprobe at the Institute of Geology, Chinese Academy of Sciences. Analytical conditions were similar to those described by Ding *et al.* (2003).

Downloaded from http://petrology.oxfordjournals.org/ at Pendlebury Library of Music on November 16, 2014

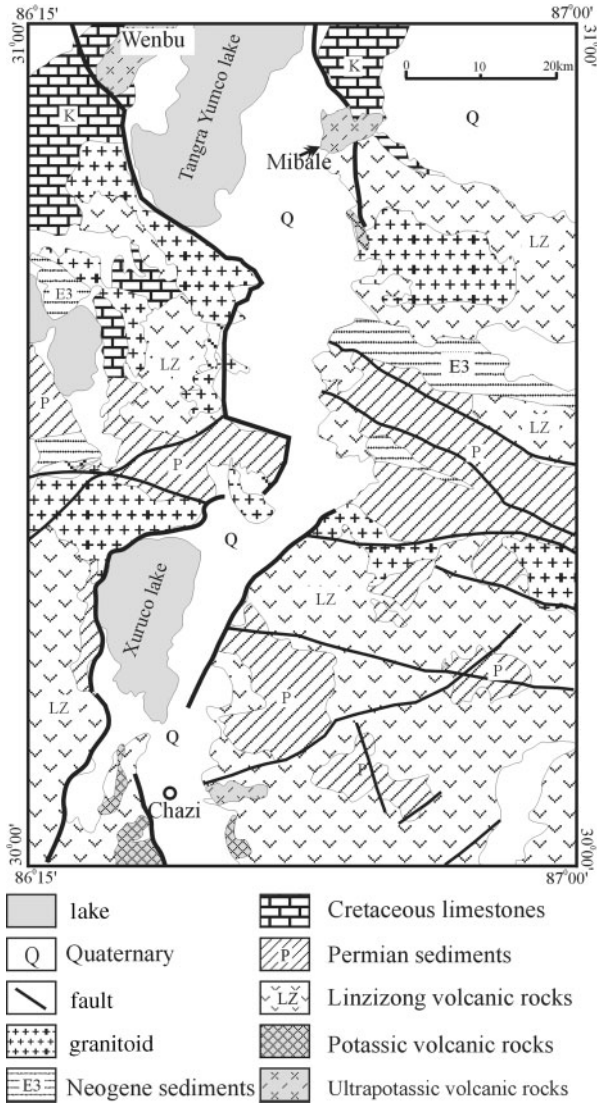


Fig. 2. Simplified geological map of the Tangra Yumco–Xuruco rift in the Lhasa terrane (modified from the Cuoqin geological map, Xizang Bureau of Geology and Mineral Resources, 2002).

PETROGRAPHY AND MINERAL CHEMISTRY

All the ultrapotassic–potassic rocks from Mibale and Chazi are highly porphyritic with phenocrysts of 1–3 mm dimension. The petrography of the ultrapotassic lavas is summarized in Table 1. The lavas are characterized by phenocrysts of phlogopite, clinopyroxene, sanidine and rare olivine, with accessory apatite and ilmenite, similar to the typical mineralogical assemblage of sanidine–phlogopite lamproites from central Italy (Conticelli & Peccerillo, 1992) and SE Spain (Venturelli *et al.*, 1984). Phlogopite and clinopyroxene are the most abundant mafic phases. The groundmass consists mainly of microcrystalline leucite, diopside, sanidine, phlogopite and varying amounts of black glass. Fe–Ti oxides with variable grain size occur as both phenocrysts and in the groundmass. All the phlogopite phenocrysts show a flow-oriented arrangement. All the samples from both Chazi and Mibale contain two generations of phlogopite. Small phlogopite I grains exhibit a distinctive erosional, 'polished' margin that is interpreted to have been caused by abrasion during turbulent magmatic emplacement. In most of the samples, phlogopite I grains are corroded and occur as cores to phlogopite II phenocrysts. Phlogopite II occurs as both large euhedral platy phenocrysts and groundmass microlites. Some of the phlogopite II phenocrysts display distinct compositional zones of oriented overgrowth on phlogopite I. Most of the phlogopite phenocrysts have a thin dark rim of fine-grained magnetite.

The two generations of phlogopite exhibit significant differences in their composition (Table 2). The distinctive compositional feature of phlogopite I is its high Ti content (6·07–8·39%), which is characteristic of lamproites (Stephen & Taylor, 1992). In contrast, phlogopite II has a lower TiO_2 content with a wider variation range (1·76–3·82 wt %), similar to the chemistry of groundmass phlogopite. Micas in the studied ultrapotassic lavas have, on average, similar Mg-number values (73–91) to phlogopites from lamproites (70–90; Conticelli & Peccerillo, 1992). In general, phlogopite II has a higher Mg-number (mostly >85) than phlogopite I (mostly <80). Both types of phlogopite have low Al_2O_3 abundances, but phlogopite I grains have distinctively lower Al_2O_3 contents (10·80–12·88 wt %) than phlogopite II grains (12·12–14·16 wt %).

The strong optical zoning from phlogopite I cores to phlogopite II rims in some phenocrysts reflects compositional variation. Most phlogopite I grains contain abundant inclusions of Ti-oxides along their cleavages. The regular orientation of the inclusions suggests that they have exsolved during cooling. The compositional variation of the phlogopite phenocrysts is broadly similar to that of micas from the Cancarix and Middle Table Mountain lamproites (Mitchell & Edgar, 2002). Experimental data (Mitchell & Edgar, 2002) indicate that these micas represent quench phases, and the micas increase their Ti contents with increasing pressure.

Most of the clinopyroxene phenocrysts are diopside–endiopside (representative compositions are given in Table 2). Individual clinopyroxene grains are typically homogeneous, but some show an increase in Mg-number from core to rim. Generally, clinopyroxene is characterized by low Ti and Al contents—a feature common to clinopyroxene in lamproites from other areas (e.g. SE Spain; Venturelli *et al.*, 1984). Pigeonite with high FeO (up to 20·9%) and K_2O contents (2%) occurs rarely. Some of the clinopyroxene phenocrysts have fine exsolution lamellae of orthopyroxene.

Downloaded from http://petrology.oxfordjournals.org/ at Pendlebury Library of Music on November 16, 2014

Table 1: Sample description of the volcanic rocks from the western Lhasa block

Location, sample no.	Lithology	Mg-no.	Phenocrysts	Groundmass
Mibale, 30°51′00″N, 86°39′26″E				
TL/10	massive lava UPV	0·73	Phl + Cpx + Ol	San + Lc + Cpx + Ilm + Ti-Mt + Ap + glass
Tl/11	massive lava UPV	0·73	Phl + Cpx + Ol	San + Lc + Cpx + Opx + Ilm + Ti-Mt + Ap + Tit
TL/18	massive lava UPV	0·64	Phl + Cpx	San + Cpx + Ilm + Ti-Mt + Ap + glass
Tl/13	massive lava UPV	0·68	Phl + Cpx + Ol	San + Cpx + Lc + Phl + Ti-Mt
Tl/03	massive lava UPV	0·67	Phl + Cpx + Ol	Cpx + San + Cpx + Lc + Phl + Ti-Mt + Ap
Tl/08	massive lava UPV	0·62	Phl + Cpx	San + Cpx + Ilm + Ti-Mt + Ap + Tit
Tl/17	massive lava UPV	0·61	Ol + Phl + Cpx	San + Cpx + Lc + Phl + Sp + Ilm + Ti-Mt
Tl/06	massive lava PVR	0·58	San + Phl + Cpx	San + Ti-Mt + Ap + glass
Tl/59	massive lava PVR	0·58	San + Phl + Cpx	San + Ti-Mt + Ap + glass
Chazi, 30°02′26″N, 86°31′49″E				
CHZ-1	massive lava UPV	0·64	Phl + Cpx	Lc + San + Cpx + Ilm + Ti-Mt + Ap + glass
CHZ-2	massive lava UPV	0·65	Cpx + Phl + Ol	San + Lc + Cpx + Phl + Ilm + Ti-Mt + Ap
CHZ-3	massive lava UPV	0·64	Cpx + Phl + Ol	Lc + San + Cpx + Ilm + Ti-Mt + Ap
CHZ-4	massive lava UPV	0·64	Phl + Cpx	San + Lc + Cpx + Ti-Mt + Ap
CHZ-5	massive lava UPV	0·63	Phl + Cpx	San + Lc + Cpx + Ti-Mt + Ap + Tit
CHZ-6	massive lava UPV	0·61	Phl + Cpx	San + Lc + Ilm + Ti-Mt + Ap
CHZ-7	massive lava UPV	0·66	Phl + Cpx + Ol	Lc + San + Ti-Mt + Ap + glass
CHZ-8	massive lava UPV	0·66	Phl + Cpx	San + Cpx + Ilm + Ti-Mt + Ap
CHZ-9	massive lava UPV	0·66	Phl + Cpx	San + Lc + Cpx + Ilm + Ti-Mt + Ap
CHZ-10	massive lava UPV	0·66	Phl + Cpx	San + Cpx + Ilm + Ti-Mt + Ap + glass
CHZ-11	massive lava UPV	0·67	Phl + Cpx + Ol	San + Lc + Cpx + Ilm + Ti-Mt + Ap
CHZ-12	massive lava UPV	0·65	Cpx + Phl	San + Lc + Cpx + Ilm + Ti-Mt + Ap

UPV, ultrapotassic; PVR, potassic; Mg-no. = $Mg/(Mg + Fe_{total})$. Phl, phlogopite; Cpx, clinopyroxene; Ol, olivine; Opx, orthopyroxene; San, sanidine; Lc, leucite; Ilm, ilmenite; Ti-Mt, Ti-magnetite; Ap, apatite; Sp, spinel; Tit, titanite.

Rare olivine occurs as small undeformed grains, and may be replaced by pseudomorphs of other silicates or carbonates. The olivine has high FeO (28·93–36·54 wt %) and low MgO contents (25·69–32·63 wt %) and Mg-number (0·55–0·67). Titaniferous magnetite is commonly the only Fe–Ti oxide phase present as phenocrysts and in the groundmass. One sample (Tl/17) has Cr-spinel grains in its groundmass. High-Cr spinels (Cr_2O_3 34·79 wt %) also occur in the Xungba ultrapotassic lavas (Miller *et al.*, 1999).

Sanidine is the sole feldspar that crystallized in these rocks. It is present as both phenocrysts and in the groundmass. Sanidine phenocrysts have an Or content range from 81·9 to 58·6%, and show an increase in Na_2O and a decrease in Or content from core to rim (Table 3). Like sanidines from lamproites of SE Spain (Venturelli *et al.*, 1984), the studied feldspars are frequently characterized by appreciable amounts of FeO and TiO_2 (FeO 0·25–1·8 wt %, TiO_2 0·07–0·49 wt %; Table 3). This is consistent with the occurrence of small Fe–Ti oxide inclusions in the feldspars.

GEOCHEMISTRY

Major and compatible trace elements

Bulk-rock major and trace element compositions for ultrapotassic lavas from the Mibale and Chazi areas are given in Table 4. Conventionally, potassic rocks are defined as those in which K_2O exceeds Na_2O (wt % or molar). Foley *et al.* (1987) defined ultrapotassic igneous rocks as having high contents of K_2O >3 wt %, MgO >3 wt %, and K_2O/Na_2O >2 (wt %). Most of the samples meet these criteria for ultrapotasic rocks. Some samples (Tl/06 and Tl/59) from Mibale have lower MgO (<3%) and higher SiO_2 contents (Table 4), and are more properly classified as potassic. The ultrapotassic lavas are characterized by low concentrations of Al_2O_3 (10·87–13·71 wt %), CaO (4·04–7·12 wt %) and Na_2O (1·33–2·78 wt %), high K_2O (except for sample Tl/10, 6·34–9·17%) and TiO_2 (1·06–1·68%), and variable SiO_2 contents (53·33–60·07 wt %). As the ultrapotassic lavas have high K_2O and low Al_2O_3 contents, they have high molar K_2O/Al_2O_3 ratios (except for sample Tl/10, 0·60–0·8) and molar $(K_2O + Na_2O)/Al_2O_3$ ratios (0·78–1·02) and

Downloaded from http://petrology.oxfordjournals.org/ at Pendlebury Library of Music on November 16, 2014

Table 2: Selected electron microprobe analyses of the phlogopites in the ultrapotassic lavas from southern Tibet

Location:	Chazi						Mibale												
Sample:	CHZ-3			CHZ-9					TI/11					TI/18					
Type:	I	I	II	II	II	II	I	I	II	II	I	I	I	I	II	II	II	II	II
SiO_2	38·25	38·80	38·26	40·74	38·64	38·52	38·61	39·06	39·55	37·93	36·97	38·70	38·58	38·42	38·46	39·43	40·33	39·46	40·44
TiO_2	6·86	6·62	3·71	1·76	2·86	3·99	8·39	6·07	3·46	3·74	6·41	7·12	7·19	6·98	3·82	3·59	3·00	2·88	2·17
Al_2O_3	12·49	12·47	12·17	12·23	12·16	12·25	12·02	11·99	13·95	13·49	12·88	12·24	10·80	12·27	11·79	11·79	14·16	13·88	12·12
Cr_2O_3	0·04	0·01	0·32	0·59	0·81	0·39	0·06	0·05	0·78	0·00	0·02	0·17	0·08	0·10	0·31	0·33	0·41	0·54	0·86
MgO	17·74	18·70	21·33	23·44	21·85	21·42	17·61	19·46	21·44	18·21	17·10	20·28	16·83	19·00	20·99	22·22	21·23	22·64	23·32
CaO	0·00	0·00	0·01	0·00	0·02	0·01	0·03	0·02	0·02	0·07	0·03	0·01	0·00	0·00	0·02	0·03	0·22	0·06	0·01
MnO	0·05	0·09	0·10	0·07	0·09	0·13	0·11	0·13	0·05	0·00	0·11	0·04	0·04	0·03	0·01	0·06	0·01	0·01	0·02
FeO	8·42	8·07	8·50	4·82	9·63	9·13	8·65	7·91	4·79	11·14	10·78	5·42	9·64	7·45	4·33	5·51	5·58	4·00	3·94
NiO	0·06	0·02	0·11	0·05	0·04	0·07	0·02	0·03	0·24	0·06									
Na_2O	0·51	0·51	0·40	0·42	0·49	0·43	0·40	0·33	0·41	0·31	0·30	0·18	0·45	0·27	0·15	0·25	0·45	0·37	0·22
K_2O	9·33	9·57	9·71	9·77	9·30	9·46	9·28	9·57	9·70	8·82	9·45	10·20	9·69	10·27	10·54	10·34	9·02	10·07	10·75
H_2O	4·06	4·11	4·08	4·15	4·12	4·13	4·12	4·11	1·99	1·93	3·54	4·25	4·67	4·12	4·25	4·11	4·13	4·18	4·16
Total	97·81	98·97	98·71	98·03	100·00	99·92	99·30	98·73	96·38	95·70	97·59	98·61	97·97	98·91	94·67	97·66	98·54	98·09	98·01
Cations on 24(O, HO) basis																			
Si	5·649	5·656	5·624	5·891	5·623	5·600	5·622	5·702	5·958	5·901	5·520	5·622	5·775	5·614	5·808	5·777	5·782	5·697	5·863
Ti	0·762	0·726	0·410	0·191	0·313	0·436	0·918	0·667	0·392	0·438	0·720	0·778	0·810	0·767	0·434	0·396	0·324	0·313	0·237
Al	2·174	2·142	2·109	2·085	2·085	2·098	2·063	2·062	2·476	2·473	2·265	2·094	1·904	2·112	2·097	2·034	2·391	2·360	2·069
Cr	0·005	0·001	0·037	0·068	0·093	0·045	0·007	0·005	0·093	0·000	0·002	0·020	0·009	0·012	0·037	0·038	0·046	0·062	0·098
Mg	3·906	4·064	4·674	5·051	4·739	4·641	3·823	4·234	4·813	4·222	3·807	4·392	3·756	4·139	4·725	4·853	4·538	4·873	5·040
Ca	0·000	0·000	0·002	0·000	0·004	0·001	0·005	0·003	0·004	0·012	0·005	0·002	0·000	0·000	0·003	0·005	0·034	0·009	0·002
Mn	0·006	0·011	0·012	0·008	0·011	0·016	0·013	0·016	0·007	0·000	0·014	0·005	0·005	0·004	0·001	0·007	0·001	0·001	0·002
Fe	1·039	0·984	1·044	0·583	1·172	1·110	1·053	0·966	0·603	1·449	1·346	0·658	1·207	0·910	0·547	0·675	0·669	0·483	0·478
Ni	0·007	0·002	0·013	0·006	0·005	0·009	0·002	0·003	0·029	0·008									
Na	0·147	0·143	0·115	0·117	0·138	0·120	0·114	0·094	0·119	0·093	0·087	0·051	0·131	0·077	0·044	0·071	0·125	0·104	0·062
K	1·757	1·781	1·821	1·802	1·726	1·754	1·724	1·782	1·864	1·751	1·800	1·890	1·850	1·915	2·030	1·933	1·650	1·855	1·988
Total	15·452	15·509	15·861	15·801	15·908	15·829	15·343	15·535	16·357	16·347	15·566	15·512	15·447	15·550	15·726	15·789	15·560	15·757	15·839
Mg-no.	78·98	80·50	81·74	89·65	80·17	80·70	78·41	81·43	88·87	74·45	73·88	86·97	75·68	81·98	89·62	87·79	87·15	90·98	91·34

variable molar K_2O/Na_2O (1·33–4·23). The lavas also have high Mg-numbers (0·58–0·73), and high Ni (124–338 ppm) and Cr (239–564 ppm) contents. Like the ultrapotassic rocks from other parts of the Lhasa block (Miller *et al.*, 1999; Williams *et al.*, 2001, 2004; Ding *et al.*, 2003; Nomade *et al.*, 2004), the studied ultrapotassic lavas display decreasing MgO and CaO contents and increasing Al_2O_3 and K_2O contents with increasing SiO_2 (Fig. 3). In general, the compatible trace elements Ni, Co, Cr, V and Sc correlate positively with MgO content or Mg-number (Fig. 4a).

Incompatible trace elements

One of the most striking features of the ultrapotassic lavas is their high incompatible trace element abundances, including large ion lithophile elements (LILE) and light rare earth elements (LREE). Their abundances reach the extreme levels typical of many lamproites. All ultrapotassic lava samples are considerably enriched in LREE (Ce: 303–490 times) relative to chondrite, whereas heavy REE (HREE) are less enriched (Yb: 4·32–10·08 times chondrite), resulting in Ce_N/Yb_N ratios that range from 35 to 101 (Table 4). All samples have similar REE patterns, which tend to flatten out in both the LREE and HREE and exhibit pronounced negative Eu anomalies (Fig. 5a and b). Similar REE patterns have been previously reported for lamproites from SE Spain (Nixon *et al.*, 1984; Contini *et al.*, 1993) and central Italy (Rogers *et al.*, 1985). Like ultrapotassic lavas from SW Tibet (Miller *et al.*, 1999), the negative Eu anomalies in the Mibale and

Downloaded from http://petrology.oxfordjournals.org/ at Pendlebury Library of Music on November 16, 2014

Table 3: Selected electron microprobe analyses of the mineral phases in the ultrapotassic lavas from southern Tibet

Sample:	TI/11	CHZ-5		CHZ-3						TI/11					
Mineral:	Ol	Ol	Ol	Cpx	Cpx	Cpx	Cpx	Cpx	Cpx	Cpx	Cpx	Cpx	Cpx	Opx	Opx
SiO_2	36·88	35·74	35·52	52·80	52·49	52·83	52·83	52·83	52·84	54·17	53·85	53·72	53·53	50·39	51·61
TiO_2	0·05	0·02	0·12	0·46	0·42	0·66	0·55	0·55	0·61	0·39	0·50	0·79	0·33	0·25	0·33
Al_2O_3	0·00	0·02	0·12	0·11	0·09	0·95	0·68	0·10	1·15	0·50	0·45	0·66	0·29	5·34	0·06
Cr_2O_3	0·03	0·11	0·08	0·02	0·17	0·08	0·10	0·31	0·13	0·04	0·03	0·11	0·06	0·00	0·10
Fe_2O_3				1·29	2·00	1·27	0·73	1·41	1·24				0·32		0·27
FeO	28·93	34·27	36·54	7·15	6·99	3·34	4·65	7·80	3·26	7·17	5·02	5·00	6·13	20·88	25·25
MnO	0·67	0·75	0·82	0·26	0·25	0·06	0·12	0·34	0·14	0·24	0·20	0·19	0·19	0·03	0·83
MgO	32·63	28·17	25·69	15·38	15·20	17·09	16·41	15·60	17·14	15·45	16·27	17·05	14·79	3·32	17·68
CaO	0·16	0·40	0·19	20·63	20·61	22·69	22·44	20·05	22·45	21·12	22·65	21·92	23·10	1·53	2·76
Na_2O	0·03	0·02	0·03	0·48	0·51	0·16	0·19	0·43	0·21	0·52	0·34	0·19	0·44	0·04	0·17
K_2O	0·02	0·03	0·03	0·01	0·00	0·00	0·00	0·00	0·00	0·00	0·01	0·09	0·01	0·02	0·01
NiO	0·25	0·14	0·09	0·06	0·04	0·06	0·03	0·04	0·03						0·08
Total	99·66	99·68	99·21	98·64	98·77	99·19	94·79	99·46	99·21	99·60	99·32	99·72	99·16	83·78	99·13
Cations on the basis of 4(Ol), 20(titanite), 6(Cpx and Opx), 3(Ilm), 4(Ti-mag), 32(Fel) oxygens															
Si	0·999	0·996	1·005	1·983	1·976	1·949	1·966	1·978	1·947	2·007	1·988	1·973	1·994	2·412	1·990
Ti	0·001	0·001	0·003	0·013	0·012	0·018	0·015	0·016	0·017	0·011	0·014	0·022	0·009	0·009	0·009
Al	0·000	0·001	0·004	0·005	0·004	0·041	0·030	0·004	0·050	0·022	0·020	0·029	0·013	0·311	0·003
Fe^{3+}				0·037	0·057	0·035	0·021	0·040	0·034	0·000	0·000	0·000	0·010	0·000	0·008
Fe^{2+}	0·655	0·799	0·865	0·225	0·220	0·103	0·145	0·244	0·101	0·222	0·155	0·158	0·190	0·836	0·814
Cr	0·001	0·002	0·002	0·002	0·001	0·002	0·001	0·000	0·004	0·001	0·001	0·003	0·002	0·000	0·003
Mn	0·015	0·018	0·020	0·008	0·008	0·002	0·004	0·011	0·004	0·008	0·006	0·006	0·006	0·001	0·027
Mg	1·317	1·170	1·083	0·861	0·853	0·940	0·910	0·871	0·941	0·853	0·895	0·934	0·821	0·237	1·016
Ca	0·005	0·012	0·006	0·830	0·831	0·897	0·895	0·804	0·886	0·838	0·896	0·863	0·922	0·078	0·114
Na	0·002	0·001	0·002	0·035	0·037	0·012	0·014	0·031	0·015	0·037	0·024	0·014	0·032	0·004	0·012
K	0·001	0·001	0·001	0·000	0·000	0·000	0·000	0·000	0·000	0·000	0·000	0·004	0·000	0·122	0·000
Ni	0·005	0·003	0·002	0·002	0·001	0·002	0·001	0·001	0·001						0·002
Cations	3·001	3·003	2·991	4·000	4·000	4·000	4·000	4·000	4·000	4·000	3·996	4·000	4·000	3·878	4·000
Mg-no.	0·668	0·594	0·556	0·767	0·755	0·872	0·846	0·754	0·875	0·793	0·852	0·855	0·804	0·221	0·553
Ab															
An															
Or															

Sample:	TI/11		TI/18			TI/11			TI/18		TI/17	
Mineral:	Ilm	Ilm	Ilm	Ilm	Ti-mag.	Tit	San	San	San	San	San	San
SiO_2	3·87	0·01	0·02	0·09	0·07	30·23	65·03	63·71	64·66	65·19	64·69	65·17
TiO_2	50·32	41·46	37·38	46·16	7·43	38·64	0·25	0·49	0·24	0·12	0·12	0·07
Al_2O_3	0·96	0·12	0·24	0·10	1·02	1·74	16·50	17·01	16·74	18·99	18·64	18·76
Cr_2O_3	0·11	0·06	0·07	0·01	0·26	0·03						
Fe_2O_3	6·89	21·00	29·74	12·03	53·49							
FeO	23·10	35·03	31·47	39·61	37·94	1·89	0·82	1·80	0·84	0·35	0·39	0·25
MnO	8·98	1·26	0·46	1·14	0·21	0·03	0·04	0·03	0·02	0·00	0·01	0·03
MgO	0·72	0·58	0·96	0·48	0·15	0·06	0·00	0·28	0·02	0·00	0·01	0·00
CaO	0·17	0·00	0·02	0·01	0·00	27·45	0·59	0·04	0·03	1·11	0·94	0·64
Na_2O	0·15	0·00	0·00	0·00	0·00	0·05	1·77	2·18	2·16	3·75	4·08	3·48
K_2O	1·02	0·00	0·00	0·01	0·01	0·01	14·44	13·15	14·60	10·28	10·38	11·08
NiO												
Total	96·29	99·52	100·4	99·64	100·58	100·13	99·44	98·69	99·31	99·79	99·26	99·48

(continued)

Downloaded from http://petrology.oxfordjournals.org/ at Pendlebury Library of Music on November 16, 2014

Table 3: Continued

Sample:	TI/11		TI/18			TI/11			TI/18		TI/17	
Mineral:	Ilm	Ilm	Ilm	Ilm	Ti-mag.	Tit	San	San	San	San	San	San
Cations on the basis of 4(Ol), 20(titanite), 6(Cpx and Opx), 3(Ilm), 4(Ti-mag), 32(Fel) oxygens												
Si	0·098	0·000	0·001	0·002	0·003	3·955	12·106	11·941	12·067	11·865	11·866	11·918
Ti	0·934	0·796	0·712	0·881	0·211	0·268	0·035	0·069	0·034	0·016	0·017	0·010
Al	0·028	0·004	0·007	0·003	0·045	3·803	3·617	3·755	3·679	4·070	4·027	4·040
Fe^{3+}	0·127	0·403	0·566	0·230	1·518							
Fe^{2+}	0·472	0·747	0·666	0·841	1·198	0·207	0·006	0·005	0·003	0·000	0·002	0·005
Cr	0·002	0·001	0·001	0·000	0·008	0·003						
Mn	0·186	0·027	0·010	0·025	0·007	0·003	0·006	0·005	0·003	0·000	0·002	0·005
Mg	0·026	0·022	0·036	0·018	0·008	0·012	0·000	0·078	0·006	0·000	0·003	0·000
Ca	0·004	0·000	0·001	0·000	0·000	3·848	0·118	0·008	0·006	0·216	0·185	0·125
Na	0·007	0·000	0·000	0·000	0·000	0·013	0·639	0·792	0·782	1·323	1·451	1·234
K	0·032	0·000	0·000	0·000	0·000	0·002	3·429	3·144	3·476	2·387	2·429	2·585
Ni												
Cations	1·963	2·000	2·000	2·000	2·998	12·114	20·078	20·074	20·184	19·930	20·040	19·955
Mg-no.												
Ab							15·3	20·1	18·3	33·7	35·7	31·3
An							2·8	0·2	0·1	5·5	4·6	3·2
Or							81·9	79·7	81·5	60·8	59·8	65·5

Chazi ultrapotassic lavas appear unrelated to plagioclase fractionation.

All the investigated ultrapotassic lava samples have high or very high abundances of Cs (4·3–52·7 ppm), Rb (391–939 ppm), Ba (2134–3931 ppm), Sr (660–1564 ppm), Th (130–224 ppm), Pb (85–166 ppm) and Zr (790–1101 ppm; Table 3). Thorium and the LILE, particularly Rb, are significantly enriched relative to high field strength elements (HFSE) and HREE. Like the ultrapotassic lavas from SW Tibet (Miller *et al.*, 1999), ultrapotassic primitive mantle-normalized abundance patterns (Fig. 5c and d) are characterized by negative Ba, Ta, Nb, Sr, P and Ti anomalies, which occur despite the high absolute abundances of these elements.

The trace element patterns are remarkably similar to those of the lamproites from SE Spain (Venturelli *et al.*, 1984) and central Italy (Conticelli & Peccerillo, 1992). They are also broadly similar to those of post-collisional potassic lavas from northern Tibet (Turner *et al.*, 1996) although negative Ba anomalies are more pronounced, and Rb and Th are far more enriched in the ultrapotassic lavas relative to the potassic lavas from northern Tibet. Low Ba/Th and pronounced negative Ba anomalies are observed in all the Mediterranean lamproite provinces (Peccerillo, 1999). The HFSE geochemistry of all the lamproite samples from this study area is characterized by less pronounced negative Nb–Ta and Ti anomalies, and more pronounced, positive, Zr and Hf anomalies (Fig. 5c and d) than those of ultrapotassic rocks from SW Tibet (Miller *et al.*, 1999). All samples show pronounced positive Pb anomalies relative to Ce and Pr (Fig. 5c and d).

Pb–Sr–Nd isotope characteristics

Lead isotope ratios were obtained for all samples, and Nd and Sr isotope data were obtained for all samples from Mibale and five representative samples from Chazi (listed in Table 5 and plotted in Figs 6 and 7).

There are several important features of the radiogenic isotope systematics. First, in all three systems, the samples have very high $^{207}Pb/^{206}Pb$, $^{208}Pb/^{206}Pb$, radiogenic Sr and unradiogenic Nd. Second, there is a clear distinction in Sr and Pb isotope composition between the Mibale and Chazi ultramafic rocks. The former have consistently lower Sr isotope initial ratios ($^{87}Sr/^{86}Sr = 0·7166–0·7258$) than the lavas from Chazi ($^{87}Sr/^{86}Sr = 0·7308–0·7363$). The Mibale lavas have higher $^{207}Pb/^{204}Pb$ (15·7709–15·8407) and lower $^{206}Pb/^{204}Pb$ (18·4590–18·5770) than the Chazi samples ($^{207}Pb/^{204}Pb = 15·6732–15·7340$; $^{206}Pb/^{204}Pb = 18·7567–18·9310$). There is no clear distinction in

Downloaded from http://petrology.oxfordjournals.org/ at Pendlebury Library of Music on November 16, 2014

Table 4: Major and trace element compositions of the ultrapotassic lavas from southern Tibet

Location:	Mibale									
Sample:	TI/10	Repeat	TI/11	TI/18	TI/13	TI/03	TI/08	TI/17	TI/06	TI/59
SiO_2	53·33		54	56·72	54·36	54·72	56·64	60·7	60·92	62·62
TiO_2	1·68		1·62	1·58	1·45	1·43	1·61	1·06	1·22	0·92
Al_2O_3	10·87		11·09	13·4	12·18	11·53	13·49	13·29	14·16	13·79
Fe_2O_3	2·64		3·59	3·34	4·59	5·05	4·56	2·37	3·11	2·25
FeO	3·22		2·22	2·42	1·68	1·58	1·4	1·98	1·05	1·42
MgO	8·13		7·74	5·13	6·34	6·6	4·65	3·47	2·74	2·57
CaO	6·69		6·83	5·27	6·74	7·06	5·42	4·04	3·26	2·58
Na_2O	2·22		1·33	2·08	2·29	2·26	2·04	2·78	2·49	2·65
K_2O	4·47		7·33	8·02	6·99	6·34	8·05	8·21	9·17	8·74
MnO	0·1		0·09	0·07	0·1	0·08	0·07	0·07	0·06	0·07
P_2O_5	0·97		0·76	0·67	0·87	0·9	0·69	0·7	0·58	0·51
LOI	4·57		2·37	0·61	1·37	1·66	0·56	0·46	0·49	0·63
CO_2	0·26		0·14	0·02	0·02	0·04	0·14	0·06	0·06	0·42
Mg-no.	0·73		0·73	0·64	0·68	0·67	0·62	0·61	0·58	0·58
Li	14·7	14·7	14·2	10·7	19·8	16·3	8·4	14·0	12·4	23·2
Be	15·8	16·2	15·2	13·9	11·1	14·2	14·4	11·3	13·1	14·9
Sc	17·3	17·5	16·9	15·0	17·6	20·3	14·8	19·5	8·7	7·7
Ti	10113	10120	9695	9977	8834	8595	9938	9476	7543	5484
V	131·3	131·0	128·0	124·3	119·7	140·0	114·3	122·3	70·6	65·0
Cr	370·0	369·6	368·6	239·1	320·9	342·8	239·2	564·6	89·4	75·9
Co	27·6	27·2	26·6	19·3	24·5	32·7	22·1	36·2	11·6	10·7
Ni	236·9	239·2	226·9	132·3	174·8	187·9	124·5	338·6	55·6	51·00
Ga	22·1	22·3	22·3	23·8	20·6	20·2	23·8	20·5	27·1	24·1
Rb	790	786	550	576	391	611	598	939	441	442
Sr	1421	1417	1564	1196	1633	1260	1207	1004	1371	930
Y	25·0	25·0	25·2	25·4	25·8	23·9	24·1	28·6	19·9	16·9
Zr	974	971	994	784	862	783	787	966	990	340
Nb	47·3	46·9	48·8	34·0	34·9	46·4	34·5	54·2	63·0	56·5
Cs	27·0	26·8	4·3	7·3	17·1	52·7	6·6	36·7	13·1	10·5
Ba	3340	3327	3931	2531	3452	3051	2537	2835	2369	2869
La	200	200	200	138	165	154	133	156	241	204
Ce	452	451	456	337	364	359	329	397	469	418
Pr	57·2	57·1	57·0	46·8	44·8	46·6	45·8	56·5	54·5	47·2
Nd	218·7	217·7	217·1	196·1	168·6	182·8	189·6	241·3	185·6	165·4
Sm	31·2	31·1	31·0	32·0	24·6	28·2	30·8	42·7	22·9	21·8
Eu	5·47	5·45	5·47	4·93	4·73	4·60	4·80	5·93	3·90	3·91
Gd	15·46	15·49	15·21	15·27	12·96	13·71	14·67	20·00	11·01	10·51
Tb	1·57	1·57	1·56	1·51	1·40	1·41	1·44	1·89	1·15	1·08
Dy	6·33	6·28	6·33	6·12	6·02	5·78	5·87	7·28	4·67	4·29
Ho	0·979	0·977	0·972	0·961	0·979	0·910	0·922	1·086	0·731	0·638
Er	2·16	2·13	2·16	2·20	2·35	2·10	2·11	2·42	1·68	1·42
Tm	0·285	0·285	0·282	0·298	0·313	0·279	0·283	0·317	0·229	0·183
Yb	1·65	1·63	1·65	1·74	1·87	1·69	1·70	1·88	1·37	1·07
Lu	0·229	0·231	0·227	0·243	0·274	0·240	0·237	0·260	0·189	0·146
Hf	26·32	26·34	26·45	21·72	23·27	21·01	21·63	27·02	25·80	12·29

(continued)

Downloaded from http://petrology.oxfordjournals.org/ at Pendlebury Library of Music on November 16, 2014

Table 4: Continued

Location:	Mibale									
Sample:	TI/10	Repeat	TI/11	TI/18	TI/13	TI/03	TI/08	TI/17	TI/06	TI/59
Ta	2·50	2·48	2·50	1·89	1·83	2·49	1·89	2·90	3·24	2·86
W	4·67	4·65	0·74	2·71	2·34	3·57	2·53	2·47	2·63	5·59
Pb	127·5	129·3	128·5	85·2	107·7	101·5	89·4	101·2	132·8	109·5
Th	130·7	130·7	131·9	150·8	112·0	183·1	152·0	224·3	145·1	153·0
U	14·0	14·0	9·6	13·7	10·9	17·0	13·6	22·0	16·0	14·5
Th/U	9·36	9·34	13·74	11·04	10·30	10·77	11·21	10·18	9·07	10·55
Nb/Ta	18·94	18·93	19·52	18·04	19·07	18·65	18·25	18·70	19·42	19·77
Y/Ho	25·58	25·59	25·96	26·43	26·39	26·23	26·13	26·31	27·19	26·51
$(Ce/Yb)_{cn}$	71·07	71·62	71·63	50·26	50·44	55·00	50·27	54·88	88·72	101·05
Dy/Yb	3·84	3·85	3·83	3·53	3·22	3·42	3·46	3·88	3·41	4·00

Location:	Chazi											
Sample:	CHZ-1	CHZ-2	CHZ-3	CHZ-4	CHZ-5	CHZ-6	CHZ-7	CHZ-8	CHZ-9	CHZ-10	CHZ-11	CHZ-12
SiO_2	54·28	54·42	55·2	54·18	54·37	55·66	54	54·15	54·07	53·9	53·5	54·58
TiO_2	1·6	1·62	1·66	1·53	1·51	1·52	1·59	1·6	1·62	1·63	1·6	1·61
Al_2O_3	12·82	12·75	12·98	13·59	13·7	13·71	12·79	12·76	12·64	12·73	12·57	12·78
Fe_2O_3	3·39	3·29	2·69	2·7	2·89	3·11	3·3	3·25	3·43	3·51	3·28	3·31
FeO	2·95	2·85	3·48	3·88	3·67	3·02	2·93	2·82	2·68	2·68	2·92	2·95
MgO	5·66	5·87	5·71	5·95	5·74	4·95	6·05	5·84	5·9	6·03	6·32	5·88
CaO	6·48	6·48	6·1	6·54	6·36	5·78	6·64	6·67	6·79	6·59	7·12	6·37
Na_2O	1·59	1·79	1·66	1·61	1·67	1·81	1·51	1·46	1·37	1·34	1·61	1·61
K_2O	8·1	7·92	8·29	7·5	7·62	8·2	8·04	8·27	8·36	8·61	7·7	8·32
MnO	0·11	0·11	0·1	0·12	0·11	0·09	0·12	0·12	0·12	0·11	0·1	0·11
P_2O_5	1·22	1·22	1·06	0·93	0·94	0·9	1·26	1·2	1·38	1·26	1·32	1·16
LOI	0·84	0·8	0·28	0·66	0·61	0·43	0·73	0·84	0·78	0·73	0·91	0·51
CO_2	0·2	0·2	0·16	0·2	0·2	0·16	0·23	0·23	0·16	0·16	0·2	0·13
Mg-no.	0·64	0·65	0·64	0·64	0·63	0·61	0·66	0·66	0·66	0·66	0·67	0·65
Li	14·6	16·1	15·1	12·9	16·7	11·1	16·4	18·5	19·7	19·4	15·7	18·7
Be	27·3	27·5	26·9	23·8	24·7	27·8	26·1	29·5	30·4	29·0	25·2	35·6
Sc	18·8	18·3	18·5	18·6	20·1	17·4	19·3	18·2	19·5	19·1	19·5	20·1
Ti	10771	10289	10146	9809	10498	10251	10816	10292	10537	10848	10210	11601
V	136·0	137·0	141·0	147·0	164·0	134·0	151·0	137·0	135·0	145·0	142·0	152·0
Cr	313·0	299·0	286·0	297·0	329·0	269·0	326·0	316·0	324·0	322·0	357·0	351·0
Co	25·9	24·1	23·8	24·8	27·0	21·7	25·0	23·6	25·3	25·7	25·8	25·7
Ni	186·0	176·0	158·0	172·0	202·0	151·0	179·0	174·0	188·0	188·0	194·0	193·0
Ga	27·9	27·2	27·4	24·9	27·0	27·4	27·0	27·1	28·0	28·1	26·6	29·4
Rb	880	702	784	712	781	785	871	564	538	529	811	795
Sr	810	798	704	660	739	688	844	1072	911	861	855	790
Y	36·1	34·9	32·2	29·6	32·9	32·7	35·5	35·4	35·6	35·5	34·5	37·4
Zr	1101	893	806	834	884	917	983	1000	935	965	749	853
Nb	73·2	68·5	66·3	54·9	57·9	70·7	65·8	73·8	70·9	75·0	50·4	80·6
Cs	22·3	25·9	15·0	24·2	32·3	26·6	22·2	13·7	15·1	17·2	20·4	16·3
Ba	2989	2939	2498	2134	2346	2151	3167	3819	3336	3263	3287	2968

(continued)

Downloaded from http://petrology.oxfordjournals.org/ at Pendlebury Library of Music on November 16, 2014

Table 4: Continued

Location:	Chazi											
Sample:	CHZ-1	CHZ-2	CHZ-3	CHZ-4	CHZ-5	CHZ-6	CHZ-7	CHZ-8	CHZ-9	CHZ-10	CHZ-11	CHZ-12
La	139	138	139	123	133	143	140	141	135	139	138	140
Ce	351	352	334	290	310	329	347	344	361	354	336	361
Pr	54·7	54·8	52·0	45·1	48·2	50·3	53·5	52·1	56·3	54·2	53·1	56·3
Nd	244·0	247·0	231·0	199·0	215·0	221·0	236·0	234·0	247·0	243·0	237·0	254·0
Sm	46·4	45·7	42·9	36·8	40·6	40·4	45·0	43·7	47·5	45·7	45·1	48·0
Eu	6·83	6·72	6·20	5·36	5·91	5·80	6·73	6·68	7·06	6·86	6·75	6·90
Gd	26·20	26·00	24·60	21·10	22·90	23·20	25·80	24·90	26·90	26·60	25·90	27·70
Tb	2·43	2·43	2·20	1·97	2·17	2·17	2·38	2·31	2·47	2·45	2·37	2·52
Dy	9·56	9·50	8·65	7·81	8·63	8·67	9·46	9·13	9·69	9·61	9·14	9·84
Ho	1·440	1·420	1·340	1·230	1·360	1·370	1·450	1·390	1·490	1·430	1·380	1·510
Er	3·33	3·24	3·01	2·86	3·12	3·12	3·24	3·21	3·29	3·34	3·16	3·47
Tm	0·406	0·389	0·373	0·345	0·403	0·397	0·393	0·391	0·4	0·404	0·377	0·422
Yb	2·43	2·36	2·27	2·13	2·40	2·33	2·34	2·30	2·36	2·31	2·15	2·50
Lu	0·327	0·317	0·306	0·295	0·341	0·329	0·331	0·321	0·318	0·315	0·298	0·351
Hf	30·10	25·00	23·30	22·80	24·20	25·80	26·60	27·20	26·20	26·50	20·60	24·40
Ta	4·06	3·90	3·77	3·21	3·37	3·62	3·59	3·72	3·88	4·17	2·70	4·54
W	4·07	4·13	3·98	6·17	5·85	5·58	3·30	4·05	5·29	4·59	2·71	1·86
Pb	166·0	116·0	81·2	82·4	105·0	158·0	150·0	166·0	110·0	144·0	125·0	147·0
Th	204·4	187·6	154·0	166·6	202·3	184·1	219·1	202·3	213·5	139·3	231·7	198·6
U	22·4	28·2	23·7	20·2	23·3	27·7	23·9	29·4	21·9	24·5	18·2	24·0
Th/U	9·13	6·65	6·51	8·25	8·69	6·66	9·19	6·88	9·74	5·70	12·74	8·29
Nb/Ta	18·03	17·56	17·59	17·10	17·18	19·53	18·33	19·84	18·27	17·99	18·67	17·75
Y/Ho	25·07	24·58	24·03	24·07	24·19	23·87	24·48	25·47	23·89	24·83	25·00	24·77
$(Ce/Yb)_{cn}$	37·43	38·65	38·13	35·28	33·47	36·59	38·43	38·76	39·64	39·71	40·50	37·42
Dy/Yb	3·93	4·03	3·81	3·67	3·60	3·72	4·04	3·97	4·11	4·16	4·25	3·94

$^{208}Pb/^{204}Pb$ or in Nd isotope composition. Additionally, there are significant covariations in Pb/Pb and in Sr vs Pb space. These characteristics are not unique to our studied sample suites but extend to all Tibetan ultapotassic and even some potassic rocks, which invites the following comparison.

In conventional Pb isotope diagrams (Fig. 6a and b), all the post-collisional ultrapotassic–potassic rocks from the Lhasa and Qiangtang blocks form three fields. The first field is defined by ultrapotassic lavas from Xungba, Wenbu and Mibale. These have low $^{206}Pb/^{204}Pb$ with a rather small variation from 18·420 to 18·603 (Fig. 6a). Their $^{207}Pb/^{204}Pb$ (15·698–15·841) and $^{208}Pb/^{204}Pb$ (39·271–40·08) ratios are very radiogenic and plot well above the sediment evolution line of Kramers & Tolstikhin (1997). The second field comprises those rocks from the central Lhasa and Qiangtang blocks, which define a Pb isotope array with a shallow slope (Fig. 6a and b). The third field, which is intermediate in composition, is defined by potassic rocks from western Lhasa.

The first group of ultrapotassic lavas defines very steep arrays in both Pb isotope diagrams. Such a steep array in uranogenic Pb space cannot be produced by the closed-system decay of U, as this would result in highly radiogenic $^{206}Pb/^{204}Pb$ ratios as well as high $^{207}Pb/^{204}Pb$ values (Nelson, 1992). It is worth noting that at the unradiogenic end, this steep trend line extends to more depleted mid-ocean ridge basalt (MORB). In fact, it merges with the shallow array of ultrapotassic–potassic rocks from the central Lhasa and Qiangtang blocks at the more depleted isotopic compositions of Eocene (48 Ma) Dazi Na-rich calc-alkaline basalts (Fig. 6a and b, Gao *et al.*, 2006). In these diagrams, the distinct steep trend may be a binary mixing line between a highly enriched source and a depleted mantle source. The principal observation to

Downloaded from http://petrology.oxfordjournals.org/ at Pendlebury Library of Music on November 16, 2014

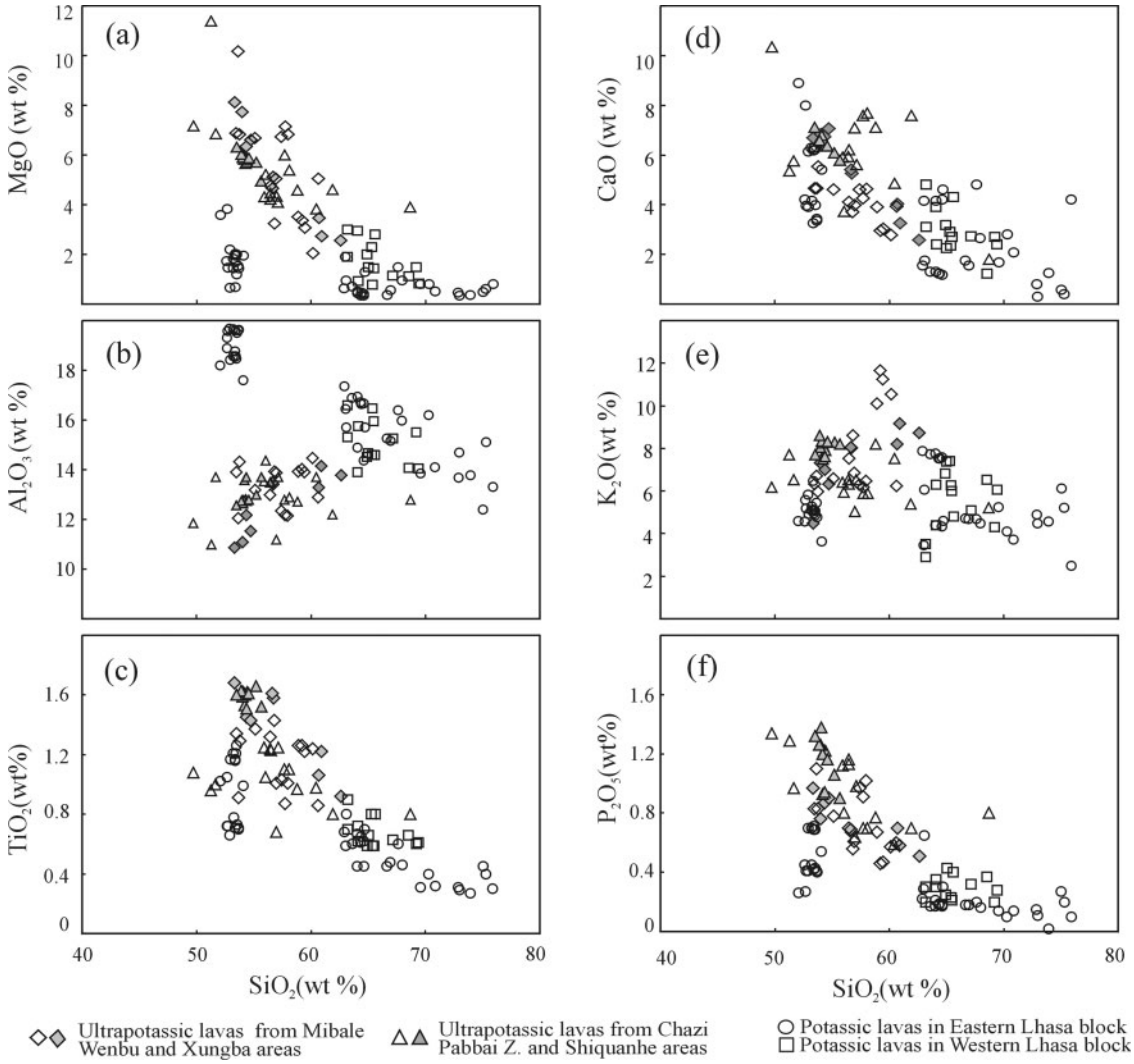


Fig. 3. Abundances of major elements (wt %) plotted against SiO_2 (wt %) for potassic and ultrapotassic rocks from the Lhasa terrane. Filled and open symbols represent, respectively, data from this study and published literature. Data sources: ultrapotassic lavas from Xungba and Jarga (Miller *et al.*, 1999), Pabbai Zong and Shiquanhe (Williams *et al.*, 2001, 2004), Wenbu (Ding *et al.*, 2003) and Zabuye (Nomade *et al.*, 2004); potassic lavas from Majiang (Turner *et al.*, 1996; Nomade *et al.*, 2004), Wuyu (Zhao *et al.*, 2001), Namling (Williams *et al.*, 2004) and Rongniduo (Coulon *et al.*, 1986; our unpublished data), Chazi (Ding *et al.*, 2003), Daggyal Tso and Shiquanhe (Williams *et al.*, 2004).

which we attach significance is that the ultrapotassic lavas from the Mibale, Xungba and Wenbu areas are isotopically unrelated to the potassic lavas from the central Lhasa and Qiangtang blocks.

The ultrapotassic rocks from the other outcrops (e.g. Pabbai Zong, Chazi and Shiquanhe) of the western Lhasa block have similar Pb isotope compositions to potassic rocks from the western Lhasa block (Fig. 6a and b). Compared with the potassic rocks of the eastern Lhasa and Qiangtang blocks, ultrapotassic–potassic rocks from the western Lhasa block have higher $^{207}Pb/^{204}Pb$ and $^{208}Pb/^{204}Pb$ ratios (Fig. 6a and b).

In Sr–Nd isotopic space, both types of the ultrapotassic samples plot in the enriched quadrant (Fig. 7) defining fields separate from the potassic rocks from central Lhasa and the Qiangtang block. The ultrapotassic lavas have highly radiogenic $^{87}Sr/^{86}Sr$ (0·7106–0·7239) and low $\varepsilon_{Nd}(t)$ ratios (−11·9 to −16·03; Miller *et al.*, 1999; Williams *et al.*, 2001; Ding *et al.*, 2003; this study). Their range overlaps with the field defined by lamproites from SE Spain (Nelson, 1992). Although all ultrapotassic–potassic volcanic rocks from the western Lhasa block have low $\varepsilon_{Nd}(t)$ ratios, their Sr isotopic compositions define a large range ($^{87}Sr/^{86}Sr$ 0·70714–0·73994). In terms of Sr isotope ratios, the ultrapotassic rocks from Chazi, Pabbai Zong and Shiquanhe overlap with potassic rocks from the western Lhasa block (Miller *et al.*, 1999; Ding *et al.*, 2003; Williams *et al.*, 2004).

Downloaded from http://petrology.oxfordjournals.org/ at Pendlebury Library of Music on November 16, 2014

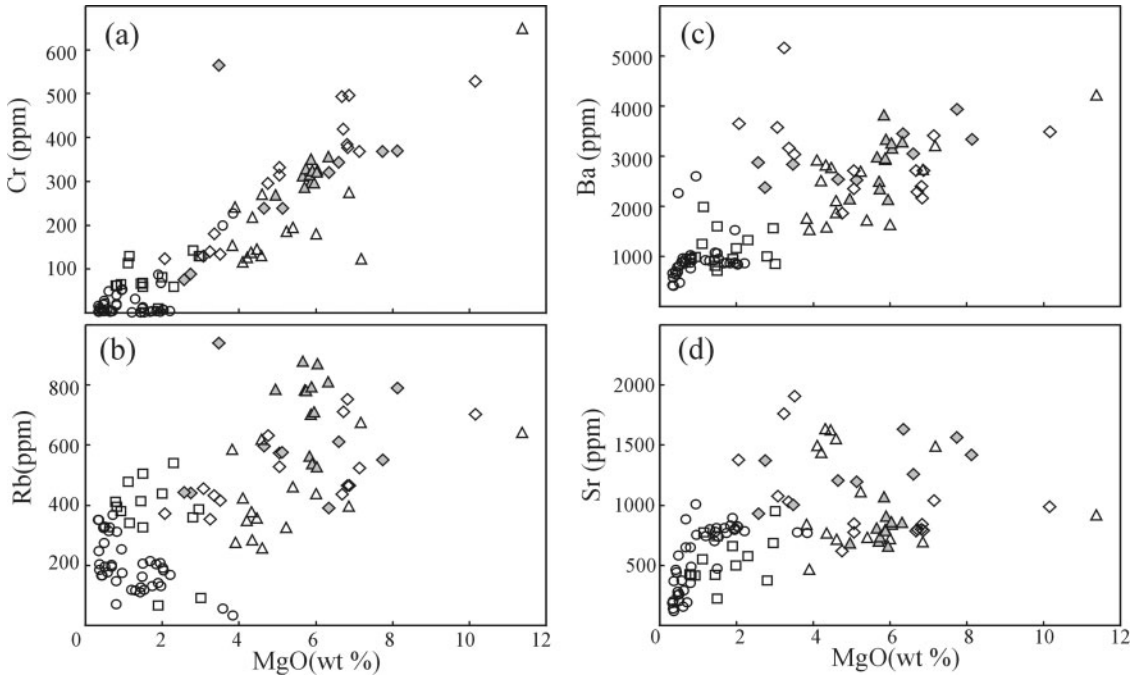


Fig. 4. Abundances of trace elements (ppm) plotted against MgO (wt %) for potassic and ultrapotassic rocks from the Lhasa terrane. Symbols and data sources as in Fig. 3.

DISCUSSION

Lamproitic affinity of ultrapotassic rocks in southern Tibet

Rocks belonging to the lamproite clan (Woolley *et al.*, 1996) exhibit a very wide range of modal mineralogy and geochemistry but may be divided into two broad types termed olivine lamproites and leucite lamproites. The latter group, also termed SiO_2-rich lamproites, is characterized by the common presence of leucite, sanidine and phlogopite, and has intermediate SiO_2 (46–60·5 wt %) and relatively low MgO (11·47–3·24 wt %) contents (Altherr *et al.*, 2004, and references therein). Table 6 lists the main geochemical characteristics of the ultrapotassic rocks from southern Tibet for comparison with lamproites from central Italy (Conticelli & Peccerillo, 1992); the compositions of the ultrapotassic lavas from the two areas are geochemically similar. Based on the classification for ultrapotassic rocks of Foley *et al.* (1987) and Foley (1992a), those from southern Tibet correspond to the chemical end-member group 1 and are therefore called leucite lamproites (Woolley *et al.*, 1996). The SiO_2 contents of the lamproite samples from the Lhasa block range from 51·27 to 60·62 wt % (Table 6) and this range generally overlaps with that of most Mediterranean occurrences, such as central Italy (56·1–58·1 wt %; Conticelli & Peccerillo, 1992) and Spain (46·1–60·5 wt %; Nixon *et al.*, 1984). Samples from southern Tibet display variable Al_2O_3 contents (10·87–14·37 wt %) resulting in CaO–Al_2O_3 characteristics that are intermediate between those of lamproite and Roman type rocks, typical of active orogenic areas (e.g. SE Spain, central Italy, NW Alps, Corsica) with variable Al_2O_3 contents (7·5–14·8). Likewise, the K_2O/Al_2O_3 ratios and TiO_2 contents of lamproites from active orogenic areas tend to be significantly lower than those of lamproites from relatively stable continental settings. In this and many other respects, the southern Tibetan ultrapotassic rocks compare closely with those from the Mediterranean 'lamproite' provinces.

Separate magma source for lamproites and evidence for binary mixing

Previous studies have suggested that post-collisional ultrapotassic rocks are temporally and spatially associated with calc-alkaline to potassic rocks in southern Tibet (Miller *et al.*, 1999; Williams *et al.*, 2001, 2004; Ding *et al.*, 2003; Nomade *et al.*, 2004; Chung *et al.*, 2005). However, it has previously been noted that the ultrapotassic lavas from the western Lhasa block exhibit some important differences in mineralogy and geochemistry from the potassic rocks of the eastern Lhasa and Qiangtang blocks (Miller *et al.*, 1999; Williams *et al.*, 2004).

In the southern Tibetan lamproites, MgO, CaO, TiO_2 and P_2O_5 are negativly correlated with SiO_2, whereas K_2O and Al_2O_3 are positivly correlated with SiO_2 (Fig. 3).

Downloaded from http://petrology.oxfordjournals.org/ at Pendlebury Library of Music on November 16, 2014

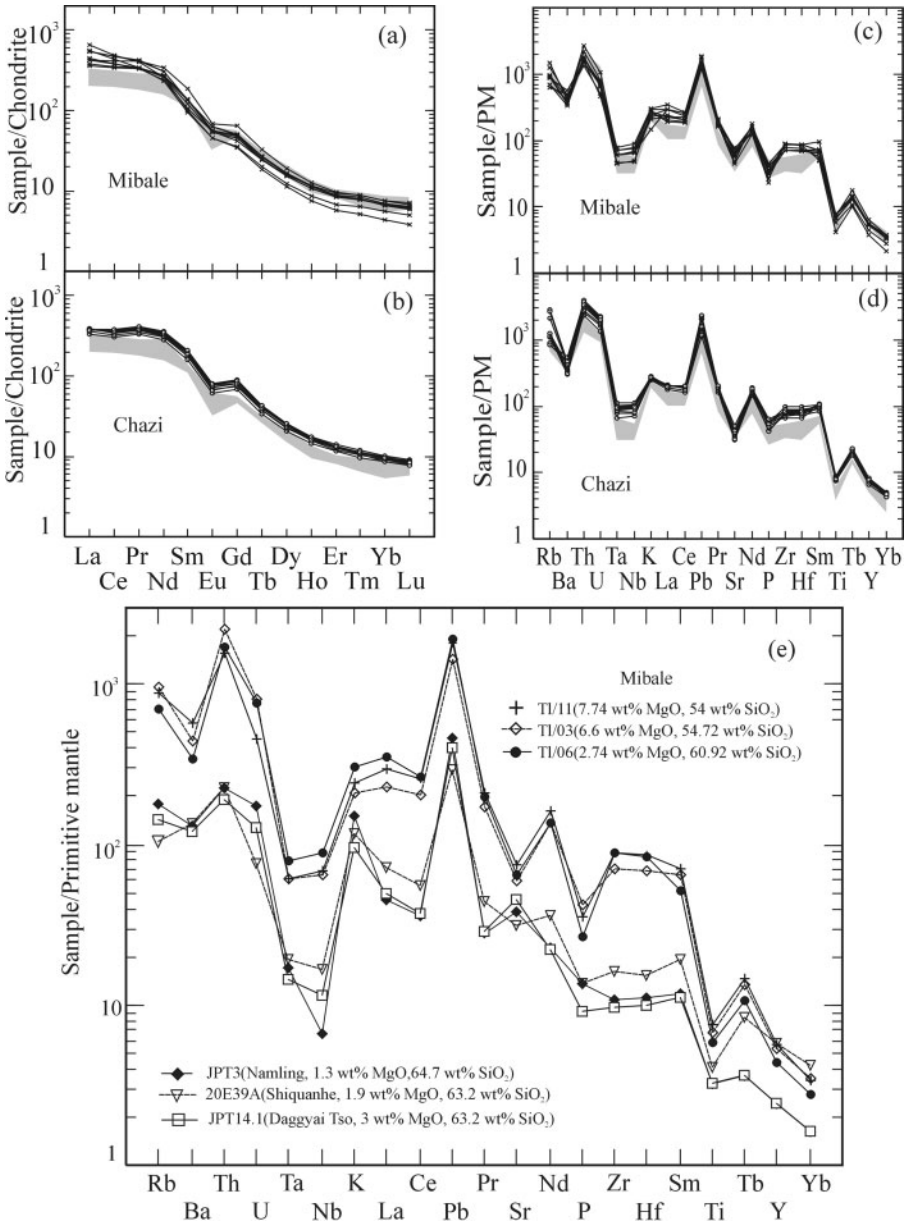


Fig. 5. Chondrite-normalized (Boynton, 1984) rare earth element diagrams for the ultrapotassic lavas from Mibale (a) and Chazi (b); primitive mantle-normalized (Sun & McDonough, 1989) trace element variation diagrams for the ultrapotassic lavas from Mibale (c) and Chazi (d), and for representative ultrapotassic samples and potassic lavas (Williams *et al.*, 2004) showing changes in the trace element pattern with MgO and SiO_2 (e). Shaded fields in (a)–(d) are the ultrapotassic lavas from Xungba, SW Tibet (Miller *et al.*, 1999).

These trends may reflect fractionation of olivine, phlogopite, clinopyroxene, spinel, apatite and Ti-bearing oxides during the petrogenesis of the lamproites. Despite this evidence for fractional crytsallization, a number of lines of evidence indicate that the potassic rocks from the eastern Lhasa block could not be generated by differentiation of parental lamproites.

First, the combined Sr and Nd isotope compositions of lamproites and potassic rocks from the eastern Lhasa and Qiangtang blocks clearly define two distinct isotopic populations (Fig. 7). The potassic lavas from the eastern Lhasa and Qiangtang terranes have relatively unradiogenic Sr and variably radiogenic Nd, resulting in a steep array, whereas the lamproites and associated potassic rocks from the western part of the Lhasa block cluster around the field of typical lamproites from other active orogenic areas (Fig. 7) with very radiogenic Sr and unradiogenic Nd.

Downloaded from http://petrology.oxfordjournals.org/ at Pendlebury Library of Music on November 16, 2014

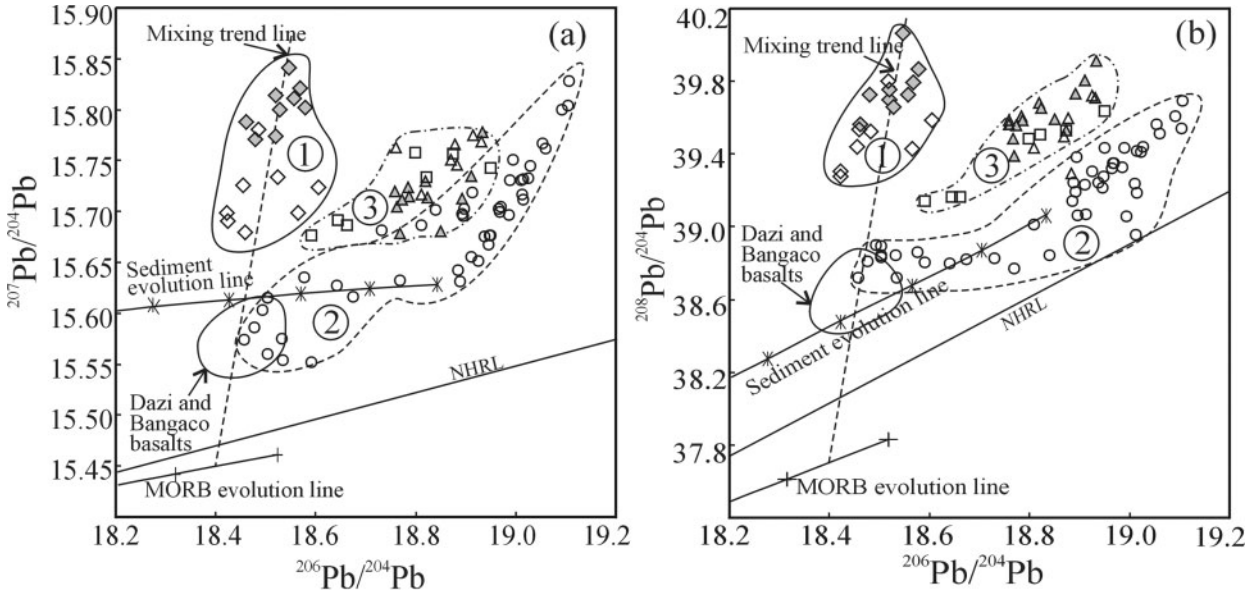


Fig. 6. Variation of $^{207}Pb/^{204}Pb$ vs $^{206}Pb/^{204}Pb$ (a) and $^{208}Pb/^{204}Pb$ vs $^{206}Pb/^{204}Pb$ (b). Compared with the potassic rocks, the ultrapotassic rocks have low $^{206}Pb/^{204}Pb$, and high $^{207}Pb/^{204}Pb$ and $^{208}Pb/^{204}Pb$. Circled numbers: (1) field for the ultrapotassic lavas from Mibale, Xungba and Wenbu areas, with low $^{206}Pb/^{204}Pb$, and high $^{207}Pb/^{204}Pb$ and $^{208}Pb/^{204}Pb$; (2) field for the ultrapotassic–potassic volcanic rocks from central Lhasa and the Qiangtang block; (3) field for the potassic rocks of the western Lhasa block. In these diagrams, Mibale ultrapotassic rocks and Dazi basalts form a binary mixing trend. This mixing line and Pb isotope array of ultrapotassic–potassic rocks from the central Lhasa and Qiangtang blocks intersect in the range of the Dazi basalts. Symbols and data sources as in Fig. 3. Sediment and MORB evolution lines from Kramers & Tolstikhin (1997). NHRL, Northern Hemisphere Reference Line.

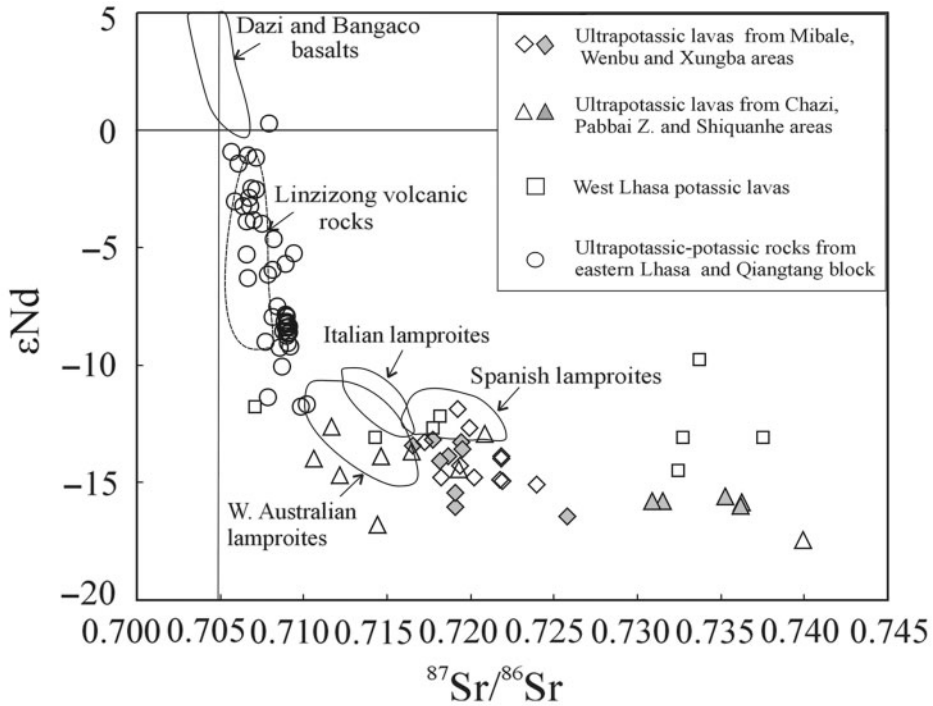


Fig. 7. $\varepsilon(t)_{Nd}$ vs $^{87}Sr/^{86}Sr$ for post-collisional ultrapotassic and potassic rocks from the Lhasa block. Data sources: ultrapotassic lavas from Xungba and Jarga (Miller *et al.*, 1999), Pabbai Zong and Shiquanhe (Williams *et al.*, 2001, 2004), Wenbu and Chazi (Ding *et al.*, 2003); western Lhasa potassic rocks from Chazi (Ding *et al.*, 2003), Daggyal Tso and Shiquanhe (Williams *et al.*, 2004); central Lhasa potassic rocks from Maquiang (Turner *et al.*, 1996), Wuyu (Zhao *et al.*, 2001), Namling (Williams *et al.*, 2004) and Rongniduo (our unpublished data); Qiangtang ultrapotassic–potassic rocks from Ding *et al.* (2003) and Guo *et al.* (2006); Bangaco and Dazi basalts from Ding *et al.* (2003) and Gao *et al.* (2006). Fields of important worldwide lamproite provinces after Nelson (1992).

Downloaded from http://petrology.oxfordjournals.org/ at Pendlebury Library of Music on November 16, 2014

Table 5: Sr, Nd and Pb isotope compositions of the ultrapotassic rocks from southern Tibet

Sample no.	$^{87}Sr/^{86}Sr \pm 2\sigma$	$^{87}Sr/^{86}Sr(I)$	$^{143}Nd/^{144}Nd \pm 2\sigma$	$^{143}Nd/^{144}Nd(I)$	$\varepsilon Nd_{(i)}$	$^{206}Pb/^{204}Pb$	$^{207}Pb/^{204}Pb$	$^{207}Pb/^{204}Pb$
Mibale								
TI/10	0·719154 ± 12	0·718719	0·511956 ± 12	0·511927	−13·88	18·55	15·84	40·06
TI/11	0·718477 ± 12	0·718202	0·511946 ± 13	0·511917	−14·07	18·52	15·81	39·70
TI/18	0·719612 ± 17	0·719132	0·511817 ± 12	0·511816	−16·04	18·52	15·77	39·75
TI/13	0·716764 ± 11	0·716577	0·511979 ± 12	0·511949	−13·44	18·46	15·79	39·56
TI/03	0·719945 ± 18	0·719468	0·511959 ± 9	0·511958	−13·27	18·56	15·81	39·72
TI/08	0·719518 ± 9	0·719131	0·51188 ± 13	0·511847	−15·44	18·48	15·77	39·72
TI/17	0·726580 ± 12	0·725848	0·511832 ± 12	0·511796	−16·43	18·58	15·80	39·86
TI/06	0·719806 ± 20	0·719503	0·511943 ± 9	0·511942	−13·58	18·57	15·82	39·79
TI/59	0·718240 ± 19	0·717776	0·511963 ± 9	0·511962	−13·19	18·53	15·80	39·65
Chazi								
CHZ-1	0·736476 ± 12	0·736289	0·511876 ± 11	0·511837	−15·62	18·77	15·68	39·48
CHZ-2						18·82	15·73	39·67
CHZ-3						18·89	15·71	39·73
CHZ-4						18·91	15·73	39·80
CHZ-5	0·730948 ± 12	0·730761	0·511866 ± 12	0·511827	−15·81	18·85	15·68	39·59
CHZ-6						18·93	15·78	39·91
CHZ-7						18·78	15·72	39·60
CHZ-8	0·731065 ± 12	0·730878	0·511867 ± 12	0·511828	−15·79	18·76	15·70	39·56
CHZ-9						18·78	15·71	39·58
CHZ-10	0·736455 ± 13	0·736268	0·511865 ± 11	0·511826	−15·83	18·77	15·71	39·56
CHZ-11						18·76	15·72	39·58
CHZ-12	0·736385 ± 12	0·736198	0·511856 ± 11	0·511817	−16·01	18·82	15·71	39·65

Both initial $^{143}Nd/^{144}Nd$ and $^{87}Sr/^{86}Sr$ ratios were corrected for an age (t) = 19 Ma. Pb isotope data are measured values.

Second, the isotopic difference also extends to the Pb isotope systematics (Fig. 6), where three different arrays can be recognized among post-collisional ultrapotassic and potassic rocks from the Lhasa terrane. The Pb isotope array for the lamproites is distinctive from that of the potassic rocks, indicating that these rocks could not be derived from each other via assimilation plus fractional crystallization (AFC) processes. Most of the mafic samples have much higher Rb content (550–880 ppm) than that of continental crust (bulk continental crust 32 ppm, upper continental crust 112 ppm; Taylor & McLennan, 1995). Thus, crustal contamination would only dilute the LILE and LREE contents of the ultrapotassic lavas. The Mibale lamproite with the most radiogenic Pb isotope signatures (sample T1/10; $^{206}Pb/^{204}Pb = 18{\cdot}518$, $^{207}Pb/^{204}Pb = 15{\cdot}841$, $^{208}Pb/^{204}Pb = 40{\cdot}058$; Table 5) is also one of the most mafic (MgO 11·8 wt %; Table 4). These isotopic arrays therefore cannot be explained by crustal contamination.

Third, some of key trace element pairs of the lamproites indicate that the lamproites have a separate magma source from the potassic rocks of the eastern Lhasa block. For example, all of the potassic rocks from the eastern Lhasa block have lower Dy/Yb and Ce/Pb and ratios than the lamproites (Fig. 8a and b). High Dy/Yb ratios of the primitive lamproites probably reflect residual garnet in the source of melting, because crystal fractionation involving garnet in the lower crust could only increase the Dy/Yb ratios of more evolved differentiation products. The difference in Ce/Pb may also be related to the sources of these magmas, indicating that the potassic rocks may have originated from a mantle region more strongly enriched with fluid. South Tibetan lamproites also exhibit very high Nb/Ta ratios (17·1–19·84), much higher than most potassic rocks (Nb/Ta = 12·66–17·2; Miller *et al.*, 1999; Zhao *et al.*, 2001; Williams *et al.*, 2004). Because Nb and Ta are not significantly decoupled during mantle melting, the distinctive high Nb/Ta ratios of the lamproites imply a special source from which this characteristic was inherited. Furthermore, the Th/La ratios, which are also robust, are high in the lamproites (0·65–1·41), ruling out significant contamination by crustal material.

Fourth, the eastern Lhasa potassic rocks and some of western Lhasa potassic rocks have lower incompatible trace element contents than the lamproites (Figs 4 and 5e). In the primitive mantle-normalized abundance diagram (Fig. 5e), these potassic rocks lack the pronounced

Downloaded from http://petrology.oxfordjournals.org/ at Pendlebury Library of Music on November 16, 2014

Table 6: Geochemical characteristics of the ultrapotassic rocks from southern Tibet, compared with those from central Italy

Location:	Central Italy[1]	Mibale	Chazi	Wenbu[2]	Pabbai Zong[3]	Xungba[4]
Rock:	LMP(3)	UPR(9)	UPR(12)	UPR(4)	UPR(4)	UPR(8)
wt %						
SiO_2	55·47–58·50	53·11–60·7	53·50–55·66	56·79–59·45	51·27–56·97	53·48–60·62
TiO_2	1·27–2·27	1·06–2·05	1·51–1·66	1·22–1·43	0·68–1·05	0·86–1·37
Al_2O_3	10·84–13·91	10·87–13·49	12·57–13·71	13·29–14·02	10·98–14·37	12·05–14·32
MgO	6·63–9·36	3·47–10·05	4·95–6·32	3·07–3·51	4·34–11·38	4·75–10·16
CaO	3·12–4·94	4·04–7·06	5·78–7·12	2·95–3·92	3·73–7·08	3·93–5·53
Na_2O	1·02–1·18	1·33–2·78	1·34–1·81	1·26–2·34	1·14–2·14	1·15–2·62
K_2O	7·46–10·73	4·47–8·63	7·5–8·61	8·62–11·66	5·03–7·69	5·98–7·54
Mg-no.	76–78	57–72	50–55	56–63	64–81	59–75
ppm						
Ba	1290–1310	1937–3677	2134–3819	3035–5160	1593–4220	2351–3488
Sr	726–803	854–1428	660–1072	1028–1907	698–1114	722–1042
Zr	655–1309	790–1012	749–1000	679–1534	253–484	387–609
Ce	257–347	203–466	290–361	507–591	123–314	185–290
Yb	1·1–2·38	1·23–1·99	2·13–2·5	1·2–2·1	1·62–2·55	1·3–2
Ce_n/Yb_n	27·69–80·24	28·94–87·24	35·28–40·50	71·58–108·95	19·39–44·06	23·53–55·57
Molar ratio						
K/Na	4·16–6·92	1·33–3·64	2·91–4·23	2·42–6·09	1·64–4·44	1·56–4·31
$(K_2O + Na_2O)/Al_2O_3$	0·74–1·22	0·78–1·02	0·79–0·92	0·99–1·14	0·69–0·93	0·74–0·86
K_2O/Al_2O_3	0·60–1·07	0·45–0·81	0·59–0·74	0·70–0·90	0·49–0·76	0·45–0·63

Sample locations and data sources: [1]Conticelli & Peccerillo (1992); [2]Ding *et al.* (2003); [3]Williams *et al.* (2001); [4]Miller *et al.* (1999).

negative Ba, Sr and P anomalies that are typical characteristics of the lamproites. Although these trace element differences could, in part, reflect different extents of fractionation, it is curious that such fractionation should have affected only some incompatible element concentrations and not others. The potassic rocks from the eastern Lhasa block have also lower incompatible trace element concentrations than any of the lamproitic samples with high MgO (Fig. 4b–d). Therefore, derivation from the lamproites through fractional crystallization alone cannot explain their trace element signatures.

Finally, there is a complete absence of lamproite contemporaneous with potassic rocks in the eastern Lhasa block, which could only be explained with preferential arrest of the hypothetical parental lamproite at depth.

In summary, the ultrapotassic rocks of lamproitic character described here differ from the more widely studied potassic rocks of eastern Lhasa and Qiangtang blocks in major, trace element and Sr–Nd–Pb isotope systematics to an extent that a separate mantle source is supported.

Of particular significance in evaluating potential mantle sources is the very steep trend in the uranogenic Pb-isotope diagram, with a slope of 0·768, corresponding to an age greater than that of the Earth (Fig. 6a and b). This is incontrovertible evidence for binary mixing. Lead isotopes cannot discriminate between mixing of two actual melts and mixing of melt sources or contamination of one melt upon ascent. However, trace element systematics, such as a positive covariation between Nb/Ta and Pb/Nd (Fig. 8e) suggest that the purest lamproites with the highest Nb/Ta were particularly enriched in Pb. The mixing hypothesis for the southern Tibetan lamproites is further corroborated by the covariations of Ba/Nb values with La/Nb values, Th/Ce values with Th/Sm and Th/U values with Cs/Rb (Fig. 8c, d and f). Together, these observations can be used to identify the nature of potential isotopic and chemical end-members.

Nature and origin of the enriched magma source component

Lamproites are known for their very unusual Sr–Nd–Pb isotopic and chemical characteristics, which, in many respects, require an incompatible element 'enriched' source (LREE, LILE, radiogenic Sr, high to extremely high $^{207}Pb/^{204}Pb$) but in others require a 'primitive' source

Downloaded from http://petrology.oxfordjournals.org/ at Pendlebury Library of Music on November 16, 2014

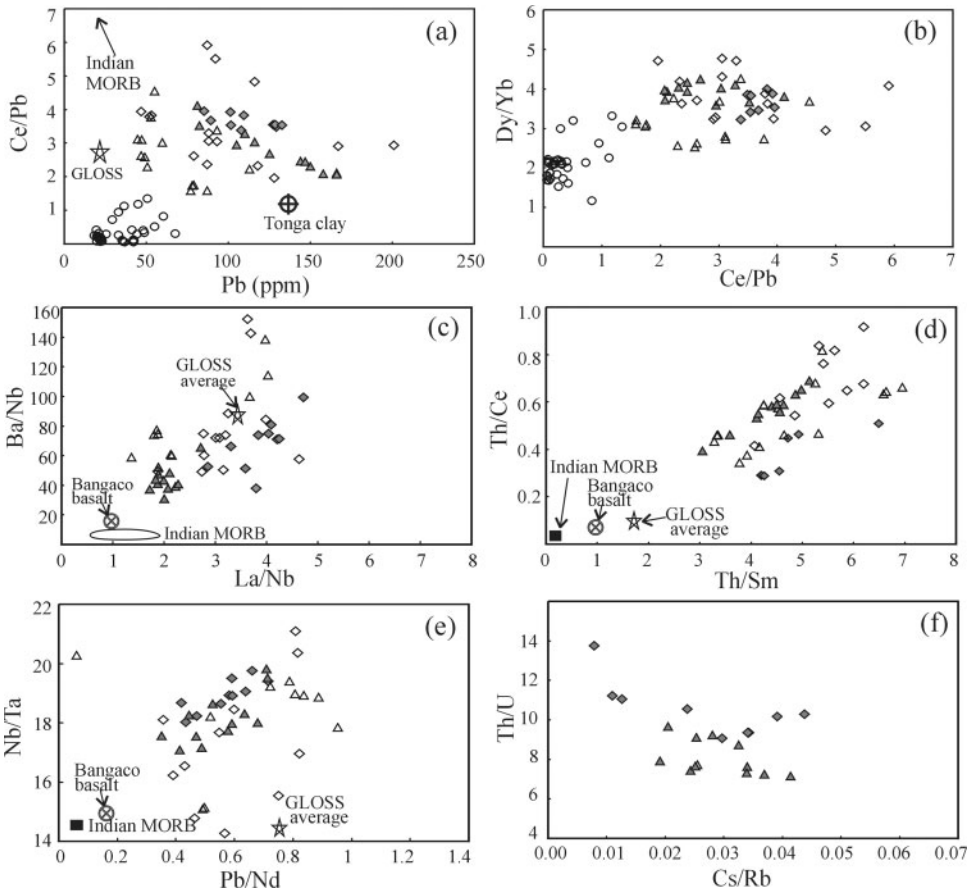


Fig. 8. Variation of Ce/Pb vs Pb (a), Dy/Yb vs Ce/Pb (b), Ba/Nb vs La/Nb (c), Th/Ce vs Th/Sm (d), Nb/Ta vs Pb/Nd (e) and Th/U vs Cs/Rb (f) for the lamproites. Data sources as in Fig. 3. Data for Indian MORB, GLOSS and Tonga clay are taken from Rehkämper & Hofmann (1997) and Plank & Langmuir (1998), respectively. Bangaco basalt from Ding *et al.* (2003). Data sources and symbols as in Fig. 3.

(e.g. high Mg-number, high compatible element content). Numerous experimental studies call for the presence of potassium-bearing minerals in the mantle source of lamproites: phlogopite and amphibole (see the review by Edgar & Vukadinovic, 1992). The incompatible trace element and Sr–Nd–Pb isotopic characteristics of most orogenic lamproites indicate that the metasomatic components in their magma source regions are principally derived from subducted lithosphere, including subducted sediments (Nelson, 1992).

Metasomatism of mantle by highly incompatible enriched fluids and melts offers the potential, first, to overwhelm the mantle's original isotopic signature and, second, to rapidly evolve radiogenic isotope ratios on account of extreme parent/daughter ratios. In the context of the studied rocks, the key question is which of these processes was responsible for the large isotopic divergence, particularly in Pb. For this purpose, we next compare lamproitic Pb isotope ratios with those of potential subducted sediment.

We recall that the Mibale, Xungba (Miller *et al.*, 1999) and Wenbu lamproites (Ding *et al.*, 2003) have low ε_{Nd} values (−12·18 to −16·03), unradiogenic $^{206}Pb/^{204}Pb$ ratios (18·45–18·56), together with high $^{207}Pb/^{204}Pb$ (15·679–15·841), $^{208}Pb/^{204}Pb$ ratios (39·557–40·058) and $^{208}Pb^*/^{206}Pb^*$ (1·075–1·145). In the Pb isotope diagrams (Fig. 9), it can easily be seen that the lamproites are higher in $^{207}Pb/^{204}Pb$ and $^{208}Pb/^{204}Pb$ but lower in $^{206}Pb/^{204}Pb$, compared with modern (granite-derived) feldspars from the Indus River system (Clift *et al.*, 2002). They correspond much better to Indian Ocean turbidites (Hemming & McLennan, 2001). In the $^{207}Pb/^{204}Pb$ vs $^{208}Pb/^{204}Pb$ diagram (Fig. 9d), in particular, the lamproites and Indian Ocean turbidites overlap. Chazi (Pabbai Zong and Shiquanhe) lamproites, on the other hand, have relatively high $^{206}Pb/^{204}Pb$, and lower $^{207}Pb/^{204}Pb$ and $^{208}Pb/^{204}Pb$ (Figs 6 and 9a, b). These lamproites overlap with the Indus River sediments and some Indian Ocean turbidites in Pb isotope space (Fig. 9). Hence the large variation in Pb isotope compositions of the two lamproite suite could

Downloaded from http://petrology.oxfordjournals.org/ at Pendlebury Library of Music on November 16, 2014

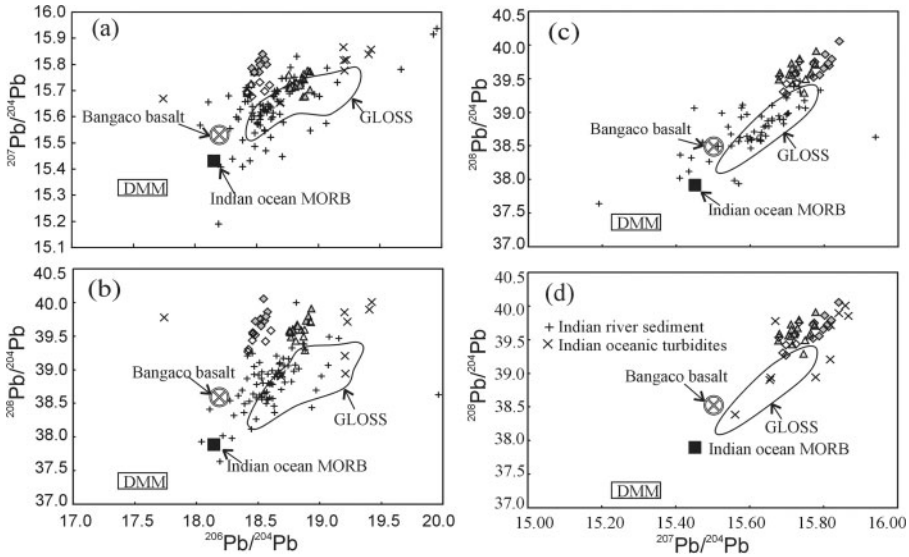


Fig. 9. Variation of $^{207}Pb/^{204}Pb$ vs $^{206}Pb/^{204}Pb$ (a), $^{208}Pb/^{204}Pb$ vs $^{206}Pb/^{204}Pb$ (b) and $^{208}Pb/^{204}Pb$ vs $^{207}Pb/^{204}Pb$ (c, d) for the southern Tibetan lamproites, Indian river sediments and Indian oceanic turbidites. Indian river sediments from Clift *et al.* (2002); Indian deep-sea turbidites from Hemming & McLennan (2001); depleted mantle (DMM) from Hofmann (1997); other data sources and symbols as in Figs 3 and 8.

be entirely accounted for by inheritance from Tethyan oceanic sediments.

For those samples of Mibale and Chazi lamproites where we have combined Pb and Nd isotope data there is also an overlap with the range of modern deep-sea turbidites (Hemming & McLennan, 2001) in the $^{208}Pb/^{204}Pb$ vs ε_{Nd} diagram (Fig. 10). Apart from those samples with $\varepsilon_{Nd} < -20$, modern deep-sea turbidites show a negative correlation between $^{208}Pb/^{204}Pb$ ratios and ε_{Nd}, clearly related to the age of the continental sediment sources (Hemming & McLennan, 2001). If the high $^{208}Pb/^{204}Pb$ ratios and low ε_{Nd} values of the lamproites indeed indicate inheritance from a sediment-derived metasomatizing agent, then these sediments must have been derived from old continental crustal sources.

There is an extreme difference between the concentration of Pb in oceanic sediment (3·2–131 ppm; Tonga clay in Fig. 8a; Plank & Langmuir, 1998) and in primitive mantle (~0·175 ppm, Hofmann, 1988), such that the addition of a very small fraction of Pb from oceanic sediment significantly affects mantle Ce/Pb and Pb isotopic ratios, which essentially take on the Pb isotopic characteristics of the sediment (Alther *et al.*, 2004). Metasomatism can be envisaged as the interaction between a LILE-enriched fluid with ambient (often depleted) mantle peridotite (Tatsumi *et al.*, 1986). However, this mechanism cannot explain the trace element and REE characteristics of the lamproites from south Tibet. Although the lamproites have pronounced negative Nb–Ta anomalies, the high HFSE abundances (Nb 34–80 ppm, Ta 1·89–4·5 ppm, Zr 340-1100 ppm) of the lamproites appear to require addition of

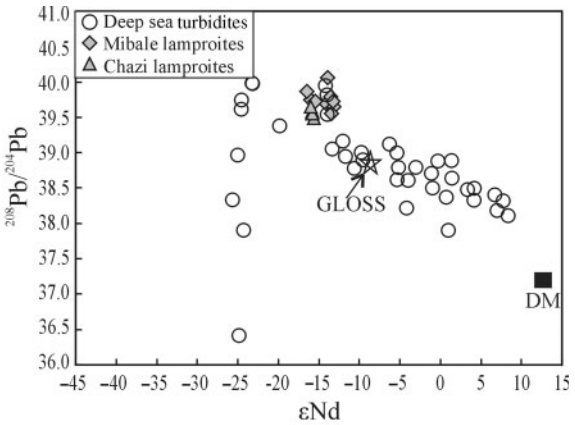


Fig. 10. $^{208}Pb/^{204}Pb$ vs $\varepsilon_{Nd}(t)$ for Tibetan lamproites. Also plotted are modern deep-sea turbidite samples from Hemming & McLennan (2001). Other data sources and symbols as in Fig. 9.

HFSE to a depleted mantle source prior to melting. HFSE addition via an aqueous fluid is generally considered unlikely because of their low solubilities in hydrous fluids (Stolz *et al.*, 1995), hence an alternative mechanism is required. This proposal is supported by the low Sr/Nd ratios (~3·1–9·7) of the south Tibetan lamproites. Experimental data indicate that Sr is more soluble in high P–T aqueous fluids than the REE (Stalder *et al.*, 1998), and elevated Sr/Nd ratios (>17; Anders & Grevesse, 1989) could be indicative of Sr addition to the arc magma source via an aqueous fluid (Kelemen *et al.*, 2003). The south Tibetan lamproites also have relatively low Ba/La ratios (~9–21) despite high Ba abundances.

Downloaded from http://petrology.oxfordjournals.org/ at Pendlebury Library of Music on November 16, 2014

This results in clear negative Ba anomalies in the primitive mantle-normalized trace element abundance pattern (Fig. 5). Elliott *et al.* (1997) proposed that high Ba/La ratios in primitive arc magmas reflect addition of an aqueous fluid component to the mantle source, whereas high Th/La ratios have been interpreted as a component derived from partial melting of subducted sediment (Elliott *et al.*, 1997; Kelemen *et al.*, 2003; Plank, 2005). The lamproites do have very high Th/La ratios (~0·6–1·4) suggesting that the Th-enriched sedimentary component in the Tibetan lamproite source was probably introduced via small-degree partial melts of subducted sediment, rather than aqueous fluids.

It is now well established that those lamproites for which high-quality trace element data exist have higher Nb/Ta ratios than MORB or continental crust (see also Murphy *et al.*, 2002). Our lamproites are no exception (Fig. 8e). Consensus is emerging that the low continental crust Nb/Ta ratio (*c.* 11–13) compared with chondrites and MORB is caused by processes in subduction zones, where Ta is preferentially transported by fluids (relative to Nb) to the melt source in which the parental continental magmas form (Stolz *et al.*, 1995; Kamber & Collerson, 2000; Kamber *et al.*, 2003). Metasomatism of refractory lithospheric mantle by infiltration of such fluids should, therefore, lead to a potential magma source with low Nb/Ta. In contrast, the residual dehydrated slab will have an elevated Nb/Ta as a result of preferential Ta loss. Stolz *et al.* (1996) interpreted the high Nb/Ta values (up to 33) of subduction-related potassic volcanic rocks as due to modification of the subarc mantle wedge by silicic melts derived from the subducting slab and its sediment veneer.

A similar situation exists with respect to Th/U. Most lamproites have unusually high Th/U ratios when compared with MORB or ocean island basalt (OIB). Lead isotope data and U-series systematics (Williams *et al.*, 1992) clearly demonstrate that this is not caused by Th/U partitioning during partial melting but is a characteristic of the source itself. The solubility of U in fluids emanating from subducted slabs is redox dependent; however, on average, Th is considered less mobile than U. Metasomatism of the mantle wedge by subduction zone derived fluids should thus lead to low Th/U sources, whereas the dehydrated slab will have a high Th/U ratio. It is important to note here that the relatively high Th/U ratio of post-Archaean upper continental crust is not a feature inherited from subduction zone processes but is caused by preferential loss of U in the weathering cycle. As a result, mature weathered sediments and red clays can acquire Th/U in excess of 10 (Plank & Langmuir, 1998).

We observe an anti-correlation between Th/U and Cs/Rb, which is also inconsistent with source metasomatism by subduction-derived fluids (Fig. 8f). Caesium is the most strongly enriched element in the continental crust and, by inference, the element most preferentially lost from dehydrated slabs, such that slab fluids are predicted to have high Cs/Rb ratios. However, our observation is that the lamproite samples with the highest Th/U have the lowest Cs/Rb ratios (Fig. 8f). Similarly, residual, partly dehydrated slabs should have comparatively low Cs/Rb ratios.

Previous studies have shown that the subduction-related magmas with a strong imprint of a partial melt or bulk melt of subducted sediment or subducted sediment itself in their source region have higher Th contents and Th/Ce ratios (Hawkesworth *et al.*, 1997*a*, 1997*b*; Elburg *et al.*, 2002; Guo *et al.*, 2006) than those related to fluid metasomatism of their mantle source. The lamproites from southern Tibet have high Th/Ce and Th/Sm ratios (Fig. 8d) as well as a high Th content. The south Tibet lamproites show positive correlations both between Th/Ce and Th/Sm (Fig. 8d) and between Ba/Nb and La/Nb (Fig. 8c). These trends could suggest simple two-component mixing. One enriched end-member in the binary mixing system could be derived from subducted sediments. The average composition of GLOSS (Plank & Langmuir, 1998) plots within the mixing trends (Fig. 8c and d). However, we note that most of the lamproite samples have higher Th/Ce, Th/Sm, Ba/Nb and La/Nb, and that they plot beyond the range of the GLOSS and Indian MORB-source mantle (Fig. 8c and d). This could either argue for a local sediment composition different from GLOSS (as inidicated by the Pb isotope compositions) and/or fractionation (i.e. amplification) of the Th/Ce and Th/Sm ratios during partial melting of subducted sediment (Guo *et al.*, 2006).

In summary, we propose that the enriched component of the Lhasa terrane lamproites can be derived from an oceanic sediment source. The trace element characteristics of the lamproites suggest that the enriched source component most probably was a partial melt derived from subducted sediment that had experienced dehydration-related preferential loss of the more fluid-mobile elements. In this model, the radiogenic Pb isotope ratios cannot be used to infer a long history of separation of the lamproite source *per se*. Rather, the complete lack of correlation between Th/U and $^{208}Pb/^{204}Pb$ ($r^2 = 0{\cdot}0089$) argues for a young age for the source, in which the isotopic characteristics were inherited from ancient (weathered) continental crustal sources stored in sediment and transported into the mantle in a subduction zone.

Depleted source component and mantle metasomatism

The suggestion of deriving lamproites from melting subducted sediment meets with the apparent problem of their high MgO and compatible trace element contents.

Downloaded from http://petrology.oxfordjournals.org/ at Pendlebury Library of Music on November 16, 2014

In the case of the Lhasa terrane lamproites, both Pb isotope and trace element systematics indicate, however, that a second end-member component, a separate melt or a contaminant was involved in their petrogenesis. In conventional Pb isotope space this component should have a much lower $^{208}Pb/^{204}Pb$ and $^{207}Pb/^{204}Pb$ than the 'enriched' end-member (Fig. 6a and b), possibly as unradiogenic as normal MORB (N-MORB). In the Dazi and Bangdaco areas, Na-rich basalts (Ding *et al.*, 2003; Gao *et al.*, 2006) are found with less radiogenic Pb isotope compositions. These were proposed to be derived from an asthenospheric mantle source beneath the Qiangtang and Lhasa terranes (Chung *et al.*, 2005; Gao *et al.*, 2006). The positively correlated array in $^{208}Pb/^{204}Pb$ vs $^{207}Pb/^{204}Pb$ (Fig. 9d) also projects to the range of composition of Indian ocean MORB (Rehkämper & Hofmann, 1997). It is therefore possible that the second (compatible element enriched) component is the depleted upper mantle.

This proposal is in agreement with trace-element ratios of similarly incompatible pairs, such as Nb/Ta, Pb/Nd, Th/Ce, Th/Sm, Ba/Nb and La/Nb, shown in Fig. 8c–e. In these diagrams, the lamproites have clear positive trends between Nb/Ta vs Pb/Nd, Th/Ce vs Th/Sm, Ba/Nb vs La/Nb. The Indian MORB (Rehkämper & Hofmann, 1997) and Bangdaco Na-rich basalts (Ding *et al.*, 2003) have the required low Nb/Ta, Pb/Nd, Th/Ce, Th/Sm, Ba/Nb and La/Nb ratios (Fig. 8c–e).

We note that Guo *et al.* (2006) recently proposed a similar origin for post-collisional, ultrapotassic and potassic rocks of the Qiangtang terrane. Their trace element modelling indicates that the mantle source of the most primitive magmas in the North Qiangtang terrane contained a high amount of subducted sediment (0·5–10%). Using a non-modal batch partial melting model (Wilson, 1989), Guo *et al.* (2006) determined that the most important factors that influence melt compositions in the envisaged environment are the degree of partial melting, the amount of subducted sediment melt added to the mantle source and the nature of residual phases in the source (e.g. phlogopite, rutile, titanite, apatite). The geochemical and mineral characteristics of the southern lamproites described here are generally consistent with the constraints of trace element modelling by Guo *et al.* (2006). According to their calculations, the proportion of subducted sediment-derived partial melt added to the mantle source ranges from 2% to around 10% for the primitive lamproite magmas studied here (Fig. 11).

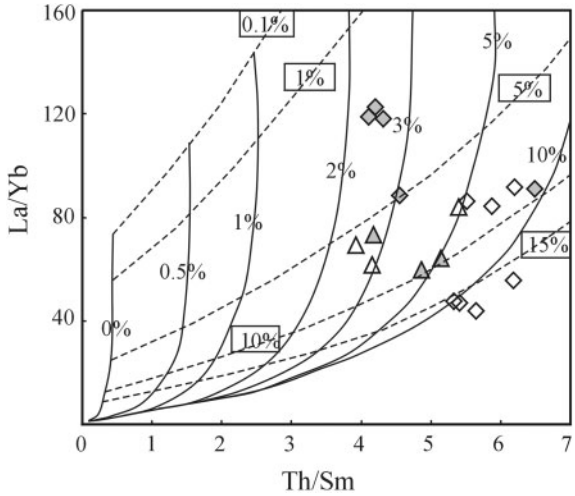


Fig. 11. La/Yb vs Th/Sm diagram for the southern Tibetan lamproites. The numbers (%) within open squares along the dashed line represent the degree of mantle partial melting. The numbers (%) along the continuous lines are the proportion of partial melt of subducted sediment in the mantle source region. These lines are the results of a non-modal batch melting model for the ultrapotassic–potassic volcanic rocks of Northern Tibet (Guo *et al.*, 2006). To minimize the effect of magmatic differentiation and crustal contamination, only primitive samples with MgO >6 wt % are plotted. Symbols as in Fig. 3.

GEODYNAMIC IMPLICATIONS

If, as we have reasoned above, the geochemical and isotopic characteristics of the Lhasa terrane lamproites originated from partial melts of subducted sediment that metasomatized the overlying depleted upper mantle (either in the lithosphere or asthenosphere), there are geodynamic implications for the post-collision tectonic evolution of the Tibetan plateau. Metasomatism by partial melts of subducted sediments is significant, even if parts of the sub-continental lithospheric mantle were enriched by aqueous fluids from slab dehydration as inferred for the source of the associated potassic magmatism (Coulon *et al.*, 1986; Turner *et al.*, 1993, 1996; Miller *et al.*, 1999; Williams *et al.*, 2001, 2004; Ding *et al.*, 2003). The separate mantle sources of the post-collisional ultrapotassic and potassic rocks (Miller *et al.*, 1999) reflect different styles of mantle source enrichment. Thus, the Precambrian Nd and Pb model ages inferred for the Tibetan mantle lithosphere by Miller *et al.* (1999) may not necessarily reflect the time when the lithosphere became isolated from asthenospheric convection, but rather the inheritance of isotopic signatures from melts derived from subducted oceanic sediments.

An important observation is that the lamproites appear to be restricted to the western part of the Lhasa block, whereas post-collisional potassic lavas occur throughout the Lhasa terrane (Nomade *et al.*, 2004). Our results indicate a coexistence of distinct domains for the post-collisional ultrapotassic–potassic volcanism in south Tibet. The along-strike variation in the post-collisional ultrapotassic–potassic volcanism in the Lhasa block, in our view, is related to a westward increase in

Downloaded from http://petrology.oxfordjournals.org/ at Pendlebury Library of Music on November 16, 2014

sediment input and the oblique subduction of the Neotethyan crust in the western Lhasa terrane. This inference was also made on the basis of a study of widespread adakite-like porphyries in southern Tibet (Gao *et al.*, 2007). Compared with adakite-like porphyries from the eastern Lhasa terrane, the mantle source of the adakite-like porphyries in the western Lhasa terrane, where lamproites occur as well, also required higher amounts of subducted sediment (Gao *et al.*, 2007).

In the convective thinning model (Turner *et al.*, 1996; Williams *et al.*, 2001, 2004), a substantial part of the lower sub-continental lithospheric mantle must have been removed before the initiation of the ultrapotassic–potassic volcanism in south Tibet. In fact, the eruption age (25–18 Ma) of the lamproites is the oldest of a period of renewed magmatic activity ~10 Myr after the end of the subduction-related magmatism in southern Tibet (Mahéo *et al.*, 2002), and the Lhasa terrane lamproitic volcanism may represent the initiation of the process of convection removal of sub-continental lithospheric mantle. If this inference is correct, removal of a substantial part of the lower sub-continental lithospheric mantle is not necessary at the onset of the lamproitic magmatism (25 Ma), because depleted asthenosphere itself is a valid end-member of two-component mixing for the lamproite magmas.

ACKNOWLEDGEMENTS

This project is financially supported by the National Key Basic Research Project (No. 2002 CB 412600) and National Natural Science Foundation of China (40672042). We thank Prelevic Dejian, Zhengfu Guo and an anonymous reviewer for their constructive reviews.

REFERENCES

Altherr, R., Meyer, H. P., Holl, A., Volker, F., Alibert, C., McCulloch, M. T. & Majer, V. (2004). Geochemical and Sr–Nd–Pb isotopic characteristics of late Cenozoic laucite lamproites from the East European Alpine belt (Macedonia and Yugoslavia). *Contributions to Mineralogy and Petrology* **147**, 58–73.

Anders, E. & Grevesse, N. (1989). Abundances of the elements: meteoritic and solar. *Geochimica et Cosmochimica Acta* **53**, 197–214.

Arnaud, N. O., Vidal, P., Tapponnier, P., Matte, P. H. & Deng, W. M. (1992). The high K_2O volcanism of northwestern Tibet: geochemistry and tectonic implications. *Earth and Planetary Science Letters* **111**, 351–367.

Boynton, W. V. (1984). Cosmochemistry of the rare earth elements: meteorite studies. In: Henderson, P. (ed.) *Rare Earth Element Geochemistry*. Amsterdam: Elsevier, pp. 63–114.

Chung, S. -L., Chu, M. -F., Zhang, Y., Xie, Y., Lo, C.-H., Lee, T. -Y., Lan, C. -Y., Li, X., Zhang, Q. & Wang, Y. (2005). Tibetan tectonic evolution inferred from spatial and temporal variations in post-collisional magmatism. *Earth-Science Reviews* **68**, 173–196.

Clift, P. D., Lee, J., Hildebrand, P., Shimizu, N., Layne, G. D., Blusztajn, J., Blum, J. D., Garzanti, E. & Khan, A. A. (2002). Nd and Pb isotope variability in the Indus River System: implications for sediment provenance and crustal heterogeneity in the Western Himalaya. *Earth and Planetary Science Letters* **200**, 91–106.

Conticelli, S. & Peccerillo, A. (1992). Petrology and geochemistry of potassic and ultrapotassic volcanism in central Italy: petrogenesis and inferences on the evolution of the mantle sources. *Lithos* **28**, 221–240.

Contini, S., Venturelli, G., Toscani, L., Capedri, S. & Barbieri, M. (1993). Cr–Zr-armalcolite-bearing lamproites of Cancarix, SE Spain. *Mineralogical Magazine* **57**, 203–216.

Coulon, C., Maluski, H., Bollinger, C. & Wang, S. (1986). Mesozoic and Cenozoic volcanic rocks from central and southern Tibet: $^{39}Ar/^{40}Ar$ dating, petrological characteristics and geodynamic significance. *Earth and Planetary Science Letters* **79**, 281–302.

DeCellers, P. G., Robinson, D. M. & Zandt, G. (2002). Implications of shortening in the Himalayan fold–thrust belt for uplift of the Tibetan plateau. *Tectonics* **21**, 1062, doi:10.1029/2001TC001322.

Ding, L., Kapp, P., Zhong, D. L. & Deng, W. M. (2003). Cenozoic volcanism in Tibet: evidence for a transition from oceanic to continental subduction. *Journal of Petrology* **44**, 1835–1865.

Edgar, A. D. & Vukadinovic, D. (1992). Implications of experimental petrology to the evolution of ultrapotassic rocks. *Lithos* **28**, 205–220.

Elburg, M. A., Bergen, M. V., Hoogewerff, J., Foden, J., Vroon, P., Zulkarnain, I. & Nasution, A. (2002). Geochemical trends across an arc–continent collision zone: magma sources and slab-wedge transfer processes below the Pantar Strait volcanoes, Indonesia. *Geochimica et Cosmochimica Acta* **66**, 2771–2789.

Elliott, T., Plank, T., Zindler, A., White, W. & Bourdon, B. (1997). Element transport from slab to volcanic front at the Mariana Arc. *Journal of Geophysical Research* **102**, 14991–15019.

Foley, S. (1992*a*). Petrological characterization of the source components of potassic magmas: geochemical and experimental constraints. *Lithos* **28**, 187–204.

Foley, S. F., Venturelli, G., Green, D. H. & Toscani, L. (1987). The ultrapotassic rocks: characteristics, classification and constraints for petrogenetic models. *Earth-Science Reviews* **24**, 81–134.

Gao, Y. -F., Hou, Z. -Q., Wei, R. -H. & Zhao, R. -S. (2003). Post-collisional adakitic porphyries in Tibet: geochemical and Sr–Nd–Pb isotopic constraints on partial melting of oceanic lithosphere and crust–mantle interaction. *Acta Geology Sinica* **77**, 194–203.

Gao, Y. -F., Hou, Z. -Q., Wei, R. -H., Meng, X. -J. & Hu, H. -B. (2006). The geochemistry and Sr–Nd–Pb isotopes of basaltic subvolcanics from the Gangdese: contraints on depleted mantle source for post-collisional volcanisms in the Tibetan plateau. *Acta Geologica Sinica* **22**, 547–557 (in Chinese with English abstract).

Gao, Y. -F., Hou, Z. -Q., Kamber, B. S., Wei, R. -H., Meng, X. -J. & Zhao, R. -S. (2007). Adakite-like porphyries from the southern Tibetan continental collision zones: evidence for slab melt metasomatism. *Contributions to Mineralogy and Petrology* **153**, 105–120.

Guo, Z. -F., Wilson, M., Liu, J. -Q. & Mao, Q. (2006). Post-collisional, potassic and ultrapotassic magmatism of the Northern Tibetan plateau: constraints on characteristics of the mantle source, geodynamic setting and uplift mechanisms. *Journal of Petrology* **47**, 1177–1220.

Hawkesworth, C. J., Turner, S. P., McDermott, F., Peat, D. W. & van Calsteren, P. (1997a). U–Th isotopes in arc magmas: implications for element transfer from the subducted crust. *Science* **276**, 551–555.

Hawkesworth, C. J., Turner, S. P., McDermott, F., Peat, D. W. & van Calsteren, P. (1997b). Element U and Th variations in island arc magmas: implications for U-series isotopes. *Chemical Geology* **139**, 207–221.

Downloaded from http://petrology.oxfordjournals.org/ at Pendlebury Library of Music on November 16, 2014

Hemming, S. R. & McLennan, S. M. (2001). Pb isotope compositions of modern deep sea turbidites. *Earth and Planetary Science Letters* **84**, 489–503.

Hofmann, A. W. (1988). Chemical differentiation of the Earth: the relationship between mantle, continental crust, and oceanic crust. *Earth and Planetary Science Letters* **90**, 279–314.

Hofmann, A. W. (1997). Mantle geochemistry: the message from oceanic volcanism. *Nature* **385**, 219–229.

Houseman, G. A., McKenzie, D. P. & Molnar, P. (1981). Convective thinning of a thickened boundary layer and its relevance for the thermal evolution of continental convergent belts. *Journal of Geophysical Research* **86**, 6115–6132.

Kamber, B. S. & Collerson, K. D. (2000). Role of 'hidden' deeply subducted slabs in mantle depletion. *Chemical Geology* **166**, 241–254.

Kamber, B. S., Greig, A., Schoenberg, R. & Collerson, K. D. (2003). Refined solution to Earth's hidden niobium: implications for evolution of continental crust and depth of core formation. *Precambrian Research* **126**, 289–308.

Kelemen, P. B., Yogodzinski, G. M. & Scholl, D. W. (2003). Along-strike variation in the Aleutian island arc: genesis of high Mg-number andesite and implications for continental crust. In: Eiler, J. (ed.) *The Subduction Factory. Geophysical Monograph, American Geophysical Union* **138**, 223–246.

Kohn, M. & Parkinson, C. D. (2002). Petrologic case for Eocene slab breakoff during the Indo-Asian collision. *Geology* **30**, 591–594.

Kramers, J. D. & Tolstikhin, I. N. (1997). Two terrestrial lead paradoxes, forward transport modeling, core formation and the history of the continental crust. *Chemical Geology* **139**, 75–110.

Liao, S. -P., Chen, Z. -H., Luo, X. -C. & Zhou, A. -J. (2002). Discovery of leucite phonolite in the Tangra Yumco area, Tibet, and its geological significance. *Geological Bulletin of China* **21**, 735–738 (in Chinese with English abstract).

Mahéo, G., Guillot, S., Blichert-Toft, J., Rolland, Y. & Pêcher, A. (2002). Slab breakoff model for the Neogene thermal evolution of South Karakorum and South Tibet. *Earth and Planetary Science Letters* **195**, 45–58.

Meyer, B., Tapponnier, P., Bourjot, L. M., Etevier, F., Gaudemer, Y., Peltzer, G., Guo, S. & Chen, Z. (1998). Crustal thickening in Gansu–Qinghai, lithospheric mantle subduction, and oblique, strike-slip controlled growth of the Tibet plateau. *Journal of Geophysical Research* **135**, 1–47.

Miller, C., Schuster, R., Klotzli, U., Mair, V., Frank, W. & Purtscheller, F. (1999). Post-collisional potassic and ultrapotassic magmatism in SW Tibet: geochemical, Sr–Nd–Pb-O isotopic constraints for mantle source characteristics and petrogenesis. *Journal of Petrology* **40**, 1399–1424.

Mitchell, R. H. & Edgar, A. D. (2002). Melting experiments on SiO_2-rich lamproites to 6·4 GPa and bearing on the sources of lamproites magmas. *Mineralogy and Petrology* **74**, 115–128.

Molnar, P. & England, P. (1978). Active tectonics of Tibet. *Journal of Geophysical Research A: Space Physics* **83**, 5361–5375.

Murphy, D. T., Kamber, B. S. & Collerson, K. D. (2002). A refined solution to the first terrestrial Pb-isotope paradox. *Journal of Petrology* **44**, 39–53.

Nelson, D. R. (1992). Isotopic characteristics of potassic rocks: evidence for the involvement of subducted sediments in magma genesis. *Lithos* **28**, 403–420.

Nixon, P. H., Thirwall, M. F., Buckley, F. & Davies, C. J. (1984). Spanish and Western Australian lamproites: aspects of whole rock geochemistry. In: Kornprobst, J. (ed.) *Kimberlites I: Kimberlites and Related Rocks*. Elsevier: Amsterdam, pp. 285–286.

Nomade, S., Renne, P. R., Mo, X., Zhao, Z. & Zhou, S. (2004). Miocene volcanism in the Lhasa block, Tibet: spatial trends and geodynamic implications. *Earth and Planetary Science Letters* **221**, 227–243.

Peccerillo, A. (1999). Multiple mantle metasomatism in central–southern Italy: geochemical effects, timing and geodynamic implications. *Geology* **27**, 315–318.

Plank, T. (2005). Constraints from thorium/lanthanum on sediment recycling at subduction zones and the evolution of the continents. *Journal of Petrology* **46**, 921–944.

Plank, T. & Langmuir, C. H. (1998). The chemical composition of subducting sediment and its consequences for the crust and mantle. *Chemical Geology* **145**, 325–394.

Rehkämper, M. & Hofmann, A. W. (1997). Recycled ocean crust and sediment in Indian Ocean MORB. *Earth and Planetary Science Letters* **147**, 93–106.

Rogers, N. W., Hawkesworth, C. J., Parker, R. J. & Marsh, J. S. (1985). The geochemistry of potassic lavas from Vulsini, central Italy, and implications for mantle enrichment processes beneath the Roman region. *Contributions to Mineralogy and Petrology* **90**, 244–257.

Stalder, R., Foley, S. F., Brey, G. P. & Horn, I. (1998). Mineral–aqueous fluid partitioning of trace elements at 900–1200°C and 3·0–5·7 GPa: new experimental data for garnet, clinopyroxene and rutile and implications for mantle metasomatism. *Geochimica et Cosmochimica Acta* **62**, 1781–1801.

Stephen, S. & Taylor, W. R. (1992). Barium- and LREE-rich, olivine–mica-lamprophyres with affinities to lamproites, Mt. Bundey, Northern Territory, Australia. *Lithos* **28**, 303–325.

Stolz, A. J., Jochum, K. P., Hofmann, A. W. & Stettel, B. (1995). HFSE constraints on the nature of island arc and ocean island magma sources. *Terra Nova* **7**, 299–316.

Stolz, A. J., Jochum, K. P., Stettel, B. & Hofmann, A. W. (1996). Fluid- and melt-related enrichment in the subarc mantle: evidence from Nb/Ta variations in island-arc basalts. *Geology* **24**, 587–590.

Sun, S. S. & McDonough, W. F. (1989). Chemical and isotopic systematics of oceanic basalts: implications for mantle composition and processes. In: Saunders, A. D. & Norry, M. J. (eds) *Magmatism in the Ocean Basins. Geological Society, London, Specical Publications* **42**, 313–345.

Tapponnier, P., Xu, Z. Q., Roger, F., Meyer, B., Arnaud, N., Wittlinger, G. & Yang, G. S. (2001). Oblique stepwise rise and growth of the Tibet Plateau. *Science* **294**, 1671–1677.

Tatsumi, Y., Hamilton, D. L. & Nesbitt, R. W. (1986). Chemical characteristics of fluid phase released from a subducted lithosphere and origin of arc magmas: evidence from high-pressure experiments and natural rocks. *Journal of Volcanology and Geothermal Research* **29**, 293–309.

Taylor, S. R. & McLennan, S. (1995). The geochemical composition of the continental crust. *Reviews of Geophysics* **33**(2), 241–265.

Turner, S., Hawkesworth, C., Liu, J. Q., Rogers, , Kelley, N. S. & van Calsteren, P. (1993). Timing of Tibetan uplift constrained by analysis of volcanic rocks. *Nature* **364**, 50–54.

Turner, S., Arnaud, N., Liu, J. Q., Rogers, N., Hawkesworth, C., Harris, N., Kelley, S., van Calsteren, P. & Deng, W. M. (1996). Post-collision, shoshonitic volcanism on the Tibetan plataeu: implications for convective thinning of the lithosphere and the source of ocean island basalts. *Journal of Petrology* **37**, 45–71.

Venturelli, G., Capedri, S., Di Battistini, G., Crawford, A., Kogarko, L. N. & Celestini, S. (1984). The ultrapotassic rocks of southeastern Spain. *Lithos* **7**, 37–54.

Williams, H. M., Turner, S., Kelley, S. & Harris, N. (2001). Age and composition of dikes in Southern Tibet: new constraints on the timing of east–west extension and its relationship to postcollisional volcanism. *Geology* **29**, 339–342.

Downloaded from http://petrology.oxfordjournals.org/ at Pendlebury Library of Music on November 16, 2014

Williams, H. M., Turner, S., Pearce, G. A., Kelley, S. P. & Harris, N. (2004). Nature of the source regions for post-collisional, potassic magmatism in southern and northern Tibet from geochemical variations and inverse element modeling. *Journal of Petrology* **45**, 555–607.

Williams, R. W., Collerson, K. D., Gill, J. B. & Denice, C. (1992). High Th/U ratios in subcontinental lithospheric mantle–mass spectrometric measurement of Th isotopes in Gaussberg lamproites. *Earth and Planetary Science Letters* **111**, 257–268.

Wilson, M. (1989). *Igneous Petrogenesis: a Global Tectonic Approach*. London: Unwin Hyman, 466 p.

Woolley, A. R., Bergman, S. C., Edgar, A. D., LeBas, M. J., Mitchell, R. H., Rock, N. M. S. & Scott Smith, B. H. (1996). Classification of lamprophyres, lamproites, kimberlites, and the kalsilitic, melilitic and leucitic rocks. *Canadian Mineralogist* **34**, 175–186.

Yin, A. (2000). Mode of Cenozoic east–west extension in Tibet suggesting a common origin of rifts in Asia during the Indo-Asia collision. *Journal of Geophysical Research* **105**, 21745–21759.

Xizang Bureau of Geology and Mineral Resources (2002). *Regional Geology of Xizang Autonomous Region*. Beijing: Geological Publishing House (in Chinese).

Zhao, Z. -D., Mo, X., Zhang, S. -Q., Guo, T. -Y., Zhou, S., Dong, G. -C. & Wang, Y. (2001). Post-collisional magmatism in Wuyu basin, central Tibet: evidence for recycling of subducted Tethyan oceanic crust. *Science in China (D)* **44** (Supplement): 27–34.

Downloaded from http://petrology.oxfordjournals.org/ at Pendlebury Library of Music on November 16, 2014